Published April 11, 2019

Special Section: Nonuniform Flow across Vadose Zone Scales

Core Ideas

- We present a new method for the hydraulic characterization of dual-permeability soils.
- The BEST-2K method was validated with synthetic soil data.
- The BEST-2K method was also validated with real experimental data for contrasting soils.

BEST-2K Method for Characterizing Dual-Permeability Unsaturated Soils with Ponded and Tension Infiltrometers

Laurent Lassabatere,* Simone Di Prima, Sofia Bouarafa, Massimo Iovino, Vincenzo Bagarello, and Rafael Angulo-Jaramillo

This study presents a new method (BEST-2K) that extends the existing BEST methods for use in characterizing the water retention and hydraulic conductivity functions of matrix and fast-flow regions in dual-permeability soils. BEST-2K requires input information from two water infiltration experiments that are performed under ponded (Beerkan) and unsaturated (tension infiltrometer) conditions at the surface. Other required inputs include water content measurements and the traditional BEST inputs (particle size distribution and bulk density). In this study, first, a flowchart of the BEST-2K method was developed and illustrated with analytically generated data for a synthetic dual-permeability soil. Next, a sensitivity analysis was performed to assess the accuracy of BEST-2K and its sensitivity to the quality of the inputs (water contents and cumulative infiltrations, and the prior estimation of the volume ratio occupied by the fast-flow region). Lastly, BEST-2K was applied to real experimental data to characterize three soils that are prone to preferential flow. BEST-2K was found to be a particularly useful tool that combines experimental and modeling approaches for characterizing dual-permeability soils and, more generally, soils prone to preferential flows.

Abbreviations: DP, dual-permeability; PSD, particle size distribution; PTF, pedotransfer function; SP, single-permeability.

The hydraulic characterization of soils, particularly their unsaturated properties, is a prerequisite for understanding water flow in the vadose zone. Several water infiltration techniques have been developed to identify the soil hydraulic properties (Angulo-Jaramillo et al., 2016). Water infiltration techniques have several clear advantages: they are non-intrusive, do not involve sampling or disturbance of the connection to the surrounding soil environment, and can be performed relatively quickly and at reasonable costs. Among these methods, the BEST methods were developed to determine the whole set of hydraulic parameters related to the hydraulic functions, namely the water retention function that describes the soil's ability to retain water by capillarity and the unsaturated hydraulic conductivity that describes the soil's ability to allow water flow (Lassabatere et al., 2006; Yilmaz et al., 2010; Bagarello et al., 2014). These methods use raw soil data (including water contents, bulk density, and particle size distribution) and one Beerkan test (consisting of a water infiltration experiment under ponded conditions through a ring). However, these methods are suitable only for single-permeability soils, whereas many soils have been shown to have several pore structures and thus should be described using multimodal or at least dual-permeability approaches (Durner, 1994).

In this study, we introduce the BEST-2K method for the hydraulic characterization of dual-permeability (DP) soils. BEST-2K is based on the principle of the BEST method, which was developed for the hydraulic characterization of single permeability (SP) soils (Lassabatere et al., 2006). The objectives of this study were to introduce the BEST-2K framework and test it with both numerical and real experimental data. The accuracy and robustness of BEST-2K was evaluated using analytically generated (error-free) data for a synthetic dual-permeability soil. BEST-2K was then applied to real data for several types

L. Lassabatere, S. Di Prima, S. Bouarafa, and R. Angulo-Jaramillo, Univ. Lyon, Univ. Claude Bernard Lyon 1, CNRS, ENTPE, UMR5023 LEHNA, F-69518, Vaulx-en-Velin, France; M. Iovino and V. Bagarello, Dep. of Agricultural, Food and Forest Sciences, Univ. of Palermo, Viale delle Scienze, 90128 Palermo, Italy. *Corresponding author (laurent.lassabatere@entpe.fr).

Received 27 June 2018.
Accepted 7 Dec. 2018.
Supplemental material online.

Citation: Lassabatere, L., S. Di Prima, S. Bouarafa, M. Iovino, V. Bagarello, and R. Angulo-Jaramillo. 2019. BEST-2K method for characterizing dual-permeability unsaturated soils with ponded and tension infiltrometers. Vadose Zone J. 18:180124. doi:10.2136/vzj2018.06.0124

© 2019 The Author(s). This is an open access article distributed under the CC BY-NC-ND license (http://creativecommons.org/licenses/by-nc-nd/4.0/).

of soils and land management conditions, including pasture, forest, and orchards.

BEST-2K Method

BEST-2K Water Retention and Hydraulic Conductivity Functions

Dual-permeability soils are composed of two regions: a matrix flow region that hosts the smaller pores and a fast-flow region that hosts the larger pores. These regions are described as Darcean porous media with different local water retention and hydraulic conductivity functions (Fig. 1a and 1b). The bulk water content and hydraulic conductivity correspond to the summation of the contributions of the matrix and fast-flow regions, as suggested by Gerke and van Genuchten (1993) (Fig. 1c):

$$\theta_{2K}(h) = w_f \theta_f(h) + (1 - w_f)\theta_m(h) \quad [1a]$$

$$K_{2K}(\theta) = w_f K_f(\theta_f) + (1 - w_f) K_m(\theta_m) \quad [1b]$$

where θ_{2K} is the bulk volumetric water content of the DP soil, θ_f and θ_m are the local volumetric water contents in the fast-flow and matrix regions, respectively, K_{2K} is the bulk hydraulic conductivity, K_f and K_m are the local hydraulic conductivities of the fast-flow and matrix regions, respectively, and w_f is the volume fraction of the DP soil occupied by the fast-flow region. By analogy with BEST method (Lassabatere et al., 2006), both regions are assigned the van Genuchten (1980) model with the Burdine condition for the description of their water retention functions and the Brooks and Corey (1964) model for the description of their unsaturated hydraulic conductivity functions:

$$\theta_m(h) = (\theta_{s,m} - \theta_{r,m})\left[1 + \left(\frac{h}{h_{g,m}}\right)^{n_m}\right]^{-m_m} + \theta_{r,m} \quad [2a]$$

$$\theta_f(h) = (\theta_{s,f} - \theta_{r,f})\left[1 + \left(\frac{h}{h_{g,f}}\right)^{n_f}\right]^{-m_f} + \theta_{r,f} \quad [2b]$$

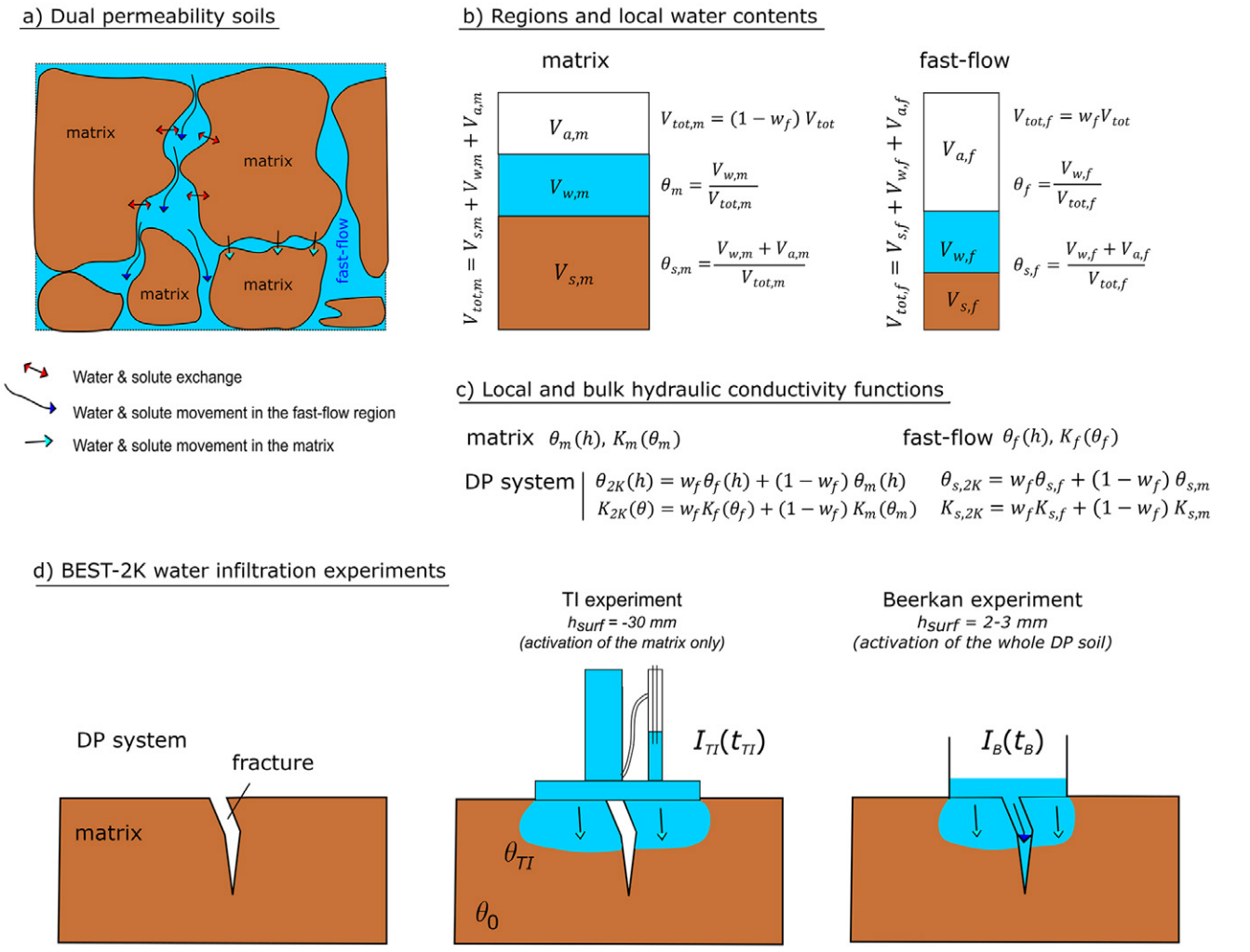

Fig. 1. Framework of (a) the dual-permeability (DP) approach (adapted from Gerke and van Genuchten, 1993), (b) regions and water contents in the DP soil, (c) 2*K* hydraulic functions of the DP soil, and (d) BEST-2K water infiltration experiments.

$$K_m(\theta_m) = K_{s,m}\left(\frac{\theta_m - \theta_{r,m}}{\theta_{s,m} - \theta_{r,m}}\right)^{\eta_m} \quad [2c]$$

$$K_f(\theta_f) = K_{s,f}\left(\frac{\theta_f - \theta_{r,f}}{\theta_{s,f} - \theta_{r,f}}\right)^{\eta_f} \quad [2d]$$

$$m_m = 1 - \frac{2}{n_m} \quad [2e]$$

$$m_f = 1 - \frac{2}{n_f} \quad [2f]$$

$$\eta_m = \frac{2}{n_m\ m_m} + 2 + p \quad [2g]$$

$$\eta_f = \frac{2}{n_f\ m_f} + 2 + p \quad [2h]$$

where m, n, and η are shape parameters, θ_r and θ_s are the residual and saturated water contents, respectively, h_g is the scale parameter for water pressure head, K_s is the saturated hydraulic conductivity, p is the tortuosity parameter fixed at 1.0 (Lassabatere et al., 2006), and subscripts m and f refer to the matrix and the fast-flow regions, respectively. Note that the subscript m refers to the matrix component of the soil, whereas the variable m refers to the shape parameter of the van Genuchten model, $m = 1 - 2/n$. BEST-2K estimates the whole set of the local hydraulic parameters for the matrix region ($\theta_{r,m}$, $\theta_{s,m}$, $h_{g,m}$, $K_{s,m}$, n_m, and η_m) and the fast-flow region ($\theta_{r,f}$, $\theta_{s,f}$, $h_{g,f}$, $K_{s,f}$, n_f, and η_f).

BEST-2K Framework

The main concept of BEST-2K involves the combination of water infiltration experiments performed at two water pressure heads: one slightly positive and the other slightly negative. These experiments quantify water infiltration when the whole pore network (both matrix and fast-flow regions) is activated and when only the matrix is activated (Fig. 1d). The contribution of the fast-flow region to water infiltration is determined by comparing the resulting cumulative infiltrations obtained from both experiments. The main inputs for BEST-2K include two water infiltration experiments (Fig. 1d): a Beerkan experiment to quantify the bulk cumulative water infiltration under ponded conditions, $I_B(t_B)$, and a tension infiltrometer (TI) experiment performed at a suction high enough to quantify the cumulative infiltration into the matrix alone, $I_{TI}(t_{TI})$. The other inputs include the initial water contents for the two tests, $\theta_{0,B}$ and $\theta_{0,TI}$, the final water content at the end of the tension infiltrometer experiment, θ_{TI}, the soil particle size distribution (PSD), and the bulk density, ρ_d, which is used to derive the bulk saturated water content, $\theta_{s,2K}$. Based on previous studies (Timlin et al., 1994), we determined that a suction of 30 mm (i.e., a water pressure head of −30 mm) is sufficient to deactivate the fast-flow region, thus restricting water flow to the matrix region, as required for the TI experiment. In fact, this threshold corresponds to the deactivation of pores with a radius >0.5 mm (Timlin et al., 1994). Practically, the value of the water pressure head could be adapted to the expected size of macropores constituting the fast-flow region.

Figure 2 illustrates the framework of the BEST-2K method. The preprocessing functions (Fig. 2, A) use the aforementioned experiments to determine the inputs, which would have been obtained with the regular Beerkan method had each region been sampled separately. Next, the regular BEST method is applied to the computed inputs to determine the hydraulic parameters for each region (Fig. 2, B). Note that the regular BEST methods used in BEST-2K are referred to as BEST-1K, in which 1K stands for single permeability, in analogy with BEST-2K in which 2K stands for dual-permeability soils. Finally, the hydraulic parameters estimated for the matrix and fast-flow regions are used to build the water retention and hydraulic conductivity functions of the DP soils (Fig. 2, C).

The following is a more detailed description of the BEST-2K method. The preprocessing functions divide the bulk PSD into two distributions, PSD_m and PSD_f, which describe the composition of the matrix and fast-flow regions, respectively. These functions use the measured water contents ($\theta_{s,2K}$, θ_{TI}, $\theta_{0,B}$, and $\theta_{0,TI}$) to derive the saturated and initial water contents for the matrix and fast-flow regions ($\theta_{s,m}$, $\theta_{0,m}$, $\theta_{s,f}$, and $\theta_{0,f}$). The preprocessing functions also use I_{TI} to compute the cumulative infiltration ($I_{B,m}$) that would have infiltrated into the matrix alone under zero water pressure head (in agreement with the Beerkan method). In this step, the inputs PSD_m, $\theta_{0,m}$, $\theta_{s,m}$, and $I_{B,m}$ for the matrix and PSD_f, $\theta_{0,f}$, and $\theta_{s,f}$ for the fast-flow region are determined (Fig. 2, arrows d_1). The set of data previously computed for the matrix (PSD_m, $\theta_{0,m}$, $\theta_{s,m}$, and $I_{B,m}$) is processed by the regular BEST method, BEST-1K, to derive the hydraulic parameters for the matrix ($\theta_{r,m}$, $\theta_{s,m}$, $h_{g,m}$, $K_{s,m}$, n_m, and η_m) (Fig. 2, d_2). Then this set of parameters is used to compute the cumulative infiltration into the matrix during the Beerkan experiment, $I_{B,m}(t_B)$, and thus its contribution to the total cumulative infiltration, I_B, to derive the cumulative infiltration into the fast-flow region, $I_{B,f}$ (Fig. 2, d_3). The $I_{B,f}$ corresponds to the cumulative infiltration that would have infiltrated into the fast-flow region on its own, under zero water pressure head (Beerkan method, Braud et al., 2005). Next, the set of data computed for the fast-flow region (PSD_f, $\theta_{0,f}$, $\theta_{s,f}$, and $I_{B,f}$) is processed by the BEST-1K method to derive the set of hydraulic parameters for the fast-flow region ($\theta_{r,f}$, $\theta_{s,f}$, $h_{g,f}$, $K_{s,f}$, n_f, and η_f) (Fig. 2, d_4). Thus, the full set of hydraulic parameters for the DP soil are obtained, and the bulk water retention and hydraulic conductivity functions can be determined.

BEST-2K Preprocessing Functions

The novelty of BEST-2K is mostly in its use of the preprocessing functions, which provide the sets of inputs PSD_m, $\theta_{0,m}$, $\theta_{s,m}$, and $I_{B,m}$ and PSD_f, $\theta_{0,f}$, $\theta_{s,f}$, and $I_{B,f}$ that are processed separately by BEST-1K. These functions are based on several

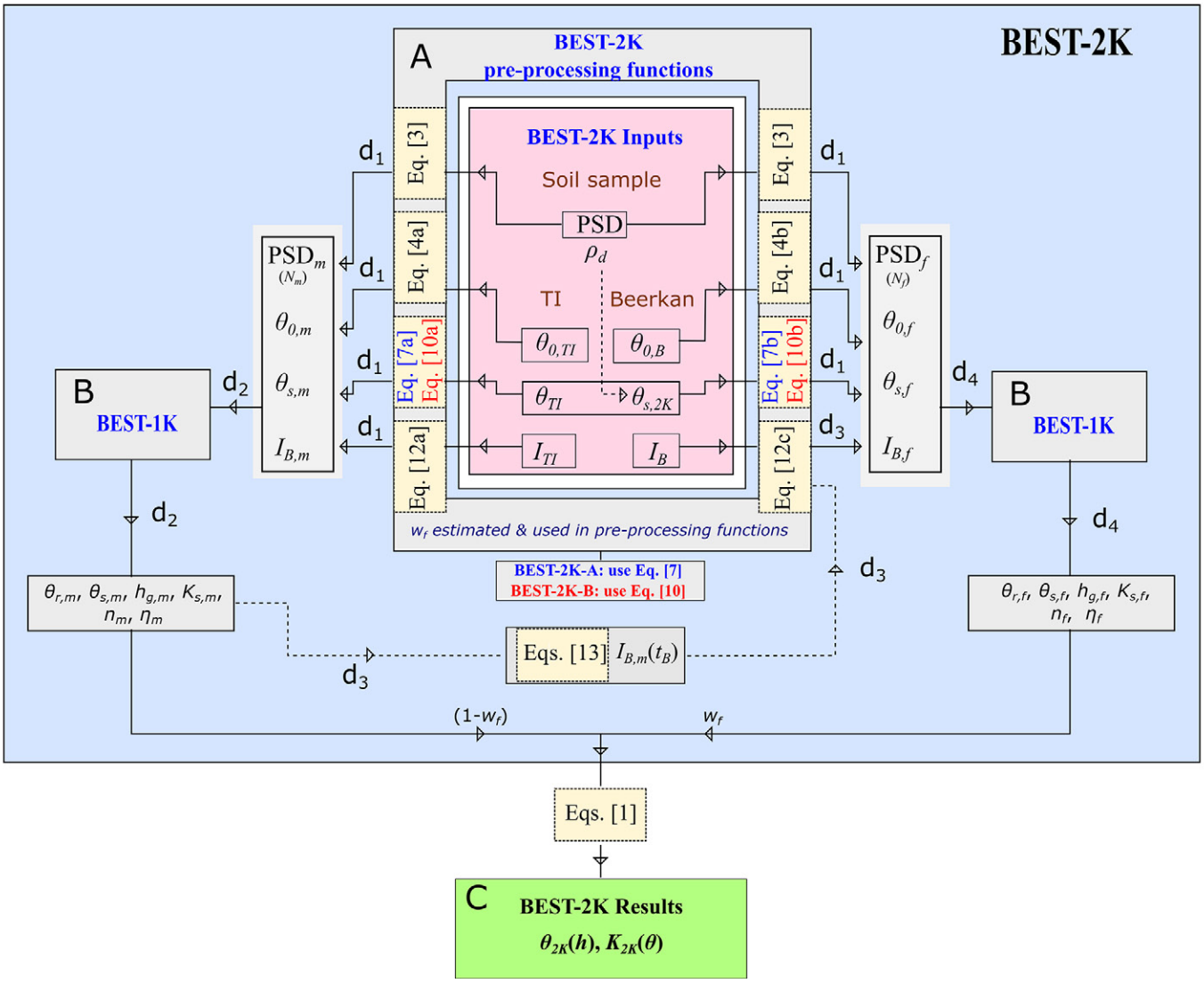

Fig. 2. Flowchart of BEST-2K method using the Beerkan and the tension infiltrometer (TI) methods. The letters A, B, C, and d_i refer to comments in the text; the uppercase letters indicate the main steps, and d_i indicate the detailed steps.

assumptions that are described and discussed below. BEST-1K is also described below and summarized in Table 1.

Particle Size Distributions

Based on the description of soils as fragmented fractal porous media, the water retention function, pore size, and PSD are expected to be consistent with one another (Rieu and Sposito, 1991). The bimodal water retention functions represent the progressive activation of the two modes of the pore size distribution. The matrix region, which is composed of small particles with small pores, may activate readily due to higher capillary forces. When the water pressure head increases enough, the larger pores of the fast-flow region may fill up and raise the water content closer to saturation. These larger pores are expected to surround the larger particles. Relationships between the water retention functions and pore size (or particle size) distributions have already been suggested (e.g., Arya and Paris, 1981). Consequently, a strong link between the bimodality of the water retention curve, the pore size distribution, and the PSD is assumed, and the following function is used to represent the bimodal PSDs:

$$FF_{2K}(D) = \tau_f \left[1 + \left(\frac{D_{g,f}}{D}\right)^{N_f}\right]^{-M_f} + (1-\tau_f)\left[1 + \left(\frac{D_{g,m}}{D}\right)^{N_m}\right]^{-M_m} \quad [3]$$

where $FF_{2K}(D)$ is the cumulative distribution of particle size, D is the particle diameter, τ_f is the fractional contribution of the particles in the fast-flow region (unknown a priori), D_g is the average diameter of either particle size mode, and N and M are textural parameters related by the expression $M = 1 - 2/N$, which is analogous to the Burdine condition. Calibration to the bulk PSD provides optimized values for N, M, and D_g, which determines

Table 1. Synthesis of BEST methods.

BEST water retention and hydraulic conductivity functions	
$\theta(h) = (\theta_s - \theta_r)[1 + (h/h_g)^n]^{-m} + \theta_r$	[t1a]
$K(\theta) = K_s[(\theta - \theta_r)/(\theta_s - \theta_r)]^{\eta}$	[t1b]
$\theta_r = 0$	[t1c]
$\theta_s = 1 - \rho_d/\rho_s$	[t1d]
$m = 1 - 2/n$	[t1e]
$\eta = 2/nm + 2 + p$ with $p = 1$	[t1f]
BEST pedotransfer functions for particle size distribution	
Fitting the particle size distribution: $FF(D) = [1 + (D_g/D)^N]^{-M}$ with $M = 1 - 2/N$	[t2]
s root of $(1 - \varepsilon)^s + \varepsilon^{2s} = 1$ with $\varepsilon = \theta_s$	[t3]
$p_m = [MN/(1 + M)](1 + \kappa)^{-1}$	[t4]
with $\kappa = (2s - 1)/[2s(1 - s)]$	[t5]
$n = 2/\{1 - (1/p_m)[\sqrt{(1 + p_m^2)} - 1]\}$	[t6]
$\eta = 2/mn + 3$	[t7]
$c_p = \Gamma(1 + 1/n)\{[\Gamma(m\eta - 1/n)/\Gamma(m\eta)] + [\Gamma(m\eta + m - 1/n)/\Gamma(m\eta + m)]\}$	[t8]
BEST analytical models	
Transient state	
$I_{O(2)}(t) = S\sqrt{t} + (AS^2 + BK_s)t$	[t9a]
$q_{O(2)}(t) = S/(2\sqrt{t}) + (AS^2 + BK_s)$	[t9b]
Steady state	
$I_{+\infty}(t) = (AS^2 + K_s)t + C(S^2/K_s)$	[t10a]
$q_{+\infty}(t) = AS^2 + K_s$	[t10b]
$A = \gamma/[r_d(\theta_s - \theta_0)]$	[t11]
$B = (1/3)(2 - \beta)[1 - (\theta_0/\theta_s)^{\eta}] + (\theta_0/\theta_s)^{\eta}$	[t12]
$C = 1/\{2[1 - (\theta_0/\theta_s)^{\eta}](1 - \beta)\}\ln(1/\beta)$	[t13]
BEST fitting algorithm for estimating sorptivity, S	
Regression of the last data points for steady state: $(t_{exp}, I_{exp})i \in \{n_{tot} - 3, ..., n_{tot}\} \rightarrow$ slope q_s^{exp} & intercept b_s^{exp}	[t14]
BEST-Steady	
$S_{best} = \sqrt{[q_s^{exp}/(A + C/b_s^{exp})]}$	[t15]
BEST-Slope & BEST-Intercept fitting procedure:	
BEST-Slope model	
$I_{O(2)}(t,S) = S\sqrt{t} + [A(1 - B)S^2 + Bq_s^{exp})]t$	[t16]
BEST-Intercept model	
$I_{O(2)}(t,S) = S\sqrt{t} + [AS^2 + BC(S^2/b_s^{exp})]t$	[t17]
$S_{opt}(k)$ minimizes $OF(S) = \sum_{i=1}^{k}\{I_{exp}(i) - I_{O(2)}[t_{exp}(i),S]\}^2$	[t18a]
$S_{best} = S_{opt}\{\max[k \mid t_{exp}(k) \le t_{max}(k)]\}$ with $t_{max}(k) = 1/[4(1 - B)^2][S_{opt}(k)/K_{s,opt}(k)]^2$	[t18b]
BEST estimation for saturated hydraulic conductivity, K_s	
$K_{s,best} = q_s^{exp} - AS_{best}^2$ BEST-Slope	[t19a]
$K_{s,best} = CS_{best}^2/b_s^{exp}$ BEST-Intercept	[t19b]
$K_{s,best} = Cq_s^{exp}/(Ab_s^{exp} + C)$ BEST-Steady	[t19c]
BEST estimation for scale parameter for water pressure head, h_g	
$h_{g,best} = S_{best}^2/\{c_p K_{s,best}(\theta_s - \theta_0)[1 - (\theta_0/\theta_s)^{\eta}]\}$	[t20]

the particle size distributions for the matrix and fast-flow regions, PSD_m and PSD_f, respectively. The textural parameters (N_m, M_m) and (N_f, M_f), which define PSD_m and PSD_f, respectively, are inputs to the BEST-1K pedotransfer functions (PTFs) that provide the shape parameters for the hydraulic functions of the matrix region (n_m, η_m) and the fast-flow region (n_f, η_f).

Initial and Saturated Water Contents

The initial water content is considered negligible in the fast-flow region, given the very little water retention by capillarity in the large pores; thus, the water remains in the matrix, occupying $1 - w_f$ of the total soil volume, leading to

$$\theta_{0,m} = \frac{\theta_{0,TI}}{1 - w_f} \quad [4a]$$

$$\theta_{0,f} = 0 \quad [4b]$$

The bulk saturated water content, $\theta_{s,2K}$, is equal to the soil porosity, which was previously derived from the soil bulk and mineral densities, ρ_d and ρ_s, respectively), as proposed by Lassabatere et al. (2006) for the BEST methods:

$$\theta_{s,2K} = 1 - \frac{\rho_d}{\rho_s} \quad [5]$$

The mineral density is often assumed to be 2.65 g cm^{-3} when no specific measurement can be obtained. To obtain the local saturated water contents, the two volumetric water contents, θ_{TI} and $\theta_{s,2K}$, are expressed as functions of the volumetric water contents in the matrix and the fast-flow regions, leading to

$$\theta_{TI} = w_f\theta_{TI,f} + (1 - w_f)\theta_{TI,m} \quad [6a]$$

$$\theta_{s,2K} = w_f\theta_{s,f} + (1 - w_f)\theta_{s,m} \quad [6b]$$

where $\theta_{TI,m}$ and $\theta_{TI,f}$ denote the local water content in the matrix and the fast-flow regions, respectively, at the end of the TI experiments. Because the tension infiltrometer deactivates the fast-flow region, we assume that no water remains in this region, i.e., $\theta_{TI,f} = 0$. We also assume that the water pressure head is sufficient to activate all the pores in the matrix region for the Beerkan and tension infiltrometer experiments; thus, $\theta_{TI,m} = \theta_{s,m}$. These hypotheses define a set of four equations with four unknowns, leading to the following equations for the saturated water contents in the matrix and fast-flow regions:

$$\theta_{s,m} = \frac{\theta_{TI}}{1 - w_f} \quad [7a]$$

$$\theta_{s,f} = \frac{\theta_{s,2K} - \theta_{TI}}{w_f} \quad [7b]$$

Given these equations, the saturated water contents are related to the volume fraction occupied by the fast-flow region, w_f; this parameter is estimated a priori. However, w_f must be chosen such that Eq. [7a–7b] predict values between zero and

one. Indeed, by definition, the water content is less than one because it is the ratio of the volume of water to the total volume of water, air, and solid. In addition, the saturated water content in the matrix region is often less than that in the fast-flow region (e.g., Gerke and van Genuchten, 1993), which leads to the following inequality:

$$\theta_{s,m} \le \theta_{s,f} < 1 \quad [8]$$

This condition, along with Eq. [7a–7b], implies the following conditions on w_f:

$$\theta_{s,2K} - \theta_{TI} \le w_f \le \frac{\theta_{s,2K} - \theta_{TI}}{\theta_{s,2K}} \quad [9]$$

The strategy outlined above defines the BEST-2K-A method. However, it relies on a very accurate measure of the difference $\theta_{s,2K} - \theta_{TI}$, which may be complicated given the uncertainty of water content measurements in the field. Consequently, a second method, BEST-2K-B, was defined based on the assumption that the saturated water contents are the same in the two regions and equal the total saturated water content, $\theta_{s,2K}$:

$$\theta_{s,f} = \theta_{s,2K} \quad [10a]$$

$$\theta_{s,m} = \theta_{s,2K} \quad [10b]$$

In this case, there is no constraint on the value of parameter w_f. Indeed, the saturated water contents are equal to the bulk saturated water content, $\theta_{s,2K}$, and do not depend on w_f. Thus, there are no risks of errors in the saturated water contents, unlike the case of BEST-2K-A, where errors can occur when Eq. [7a–7b] are calculated using erroneous values of w_f.

From a physical point of view, BEST-2K-B considers that the void ratio, i.e., the ratio of the volume of the voids to the volume of the solids, does not evolve with the particle size, meaning that the porosity remains the same in both the matrix (fine particles) and the fast-flow region (large particles). In contrast, BEST-2K-A considers that the void ratio (and thus, the porosity) may increase with the size of the particles. The fast-flow regions could also be viewed as an ensemble of capillary tubes of large dimensions with a porosity equal to one and the lack of any surrounding particles. However, such a concept is beyond this study that considers dual-permeability systems with a combination of two porous media made of voids and particles.

Cumulative Infiltration into the Matrix and Fast-Flow Regions

The cumulative infiltrations into the DP soil for both TI and Beerkan experiments, I_{TI} and I_B, respectively, correspond to the summation of the infiltrations into the matrix and fast-flow regions:

$$I_{TI} = w_f I_{TI,f} + (1 - w_f) I_{TI,m} \quad [11a]$$

$$I_B = w_f I_{B,f} + (1 - w_f) I_{B,m} \quad [11b]$$

For the TI experiment, it is assumed that water flows exclusively in the matrix and that infiltration into the fast-flow region is negligible, i.e., $I_{TI,f} = 0$. It is also assumed that water infiltration does not change appreciably between the Beerkan and TI experiments for the matrix, i.e., $I_{TI,m} = I_{B,m}$. The combination of these hypotheses with Eq. [11a] allows a direct computation of the cumulative infiltration into the matrix for the Beerkan experiments, $I_{B,m}$ (see Eq. [12a]). Then this infiltration is subtracted from the total cumulative infiltration to obtain the cumulative infiltration into the fast-flow region, $I_{B,f}$, as

$$I_{B,m} = \frac{I_{TI}}{1 - w_f} \quad [12a]$$

$$I_{B,f} = \frac{I_B - I_{TI}}{w_f} \quad [12b]$$

$$I_{B,f} = \frac{I_B - (1 - w_f) I_{B,m}(t_B)}{w_f} \quad [12c]$$

Very often, the cumulative infiltrations, $I_{TI}(t_{TI})$ and $I_B(t_B)$, are not obtained at the same times, $t_{TI} \neq t_B$. Thus, I_{TI} cannot be directly subtracted as shown in Eq. [12b]. To circumvent this inconsistency, Eq. [12c] is used to compute $I_{TI}(t_B) = (1 - w_f) I_{B,m}(t_B)$ for the time dataset t_B. The infiltration $I_{B,m}(t_B)$ is directly computed for the times t_B using the hydraulic parameters estimated for the matrix ($\theta_{r,m}$, $\theta_{s,m}$, $h_{g,m}$, $K_{s,m}$, m_m, n_m, η_m) and the quasi-exact model proposed by Haverkamp et al. (1994):

$$I_{B,m}(t_B) = I_{1D,m}(t_B) + \frac{\gamma S_m^2}{r_d \Delta\theta_m} t_B \quad [13a]$$

$$\frac{2\Delta K_m^2}{S_m^2} t_B = \frac{1}{1-\beta}\left(\frac{2\Delta K_m}{S_m^2}\left[I_{1D,m}(t_B) - K_{0,m} t_B \right] - \ln\left\{ \frac{\exp\left\{ \beta \left(2\Delta K_m / S_m^2 \right) \left[I_{1D,m}(t_B) - K_{0,m} t_B \right] \right\} + \beta - 1}{\beta} \right\} \right) \quad [13b]$$

where t_B is time for the Beerkan experiment, r_d is the radius of the disk source, $\Delta\theta_m$ ($= \theta_{s,m} - \theta_{0,m}$) is the difference between the final and initial water contents, ΔK [$= K_{s,m} - K_{0,m}$, with $K_{0,m} = K(\theta_{0,m})$] is the difference between the final and initial hydraulic conductivities, and β and γ are constants commonly set at 0.6 and 0.75, respectively (Haverkamp et al., 1994; Smettem et al., 1994). The sorptivity, S_m, can be computed from the water diffusivity, D_m, and the initial and final water contents using Parlange's approximation (Parlange, 1975):

$$S_m^2(\theta_{0,m}, \theta_{s,m}) = \int_{\theta_{0,m}}^{\theta_{s,m}} (\theta_{s,m} + \overline{\theta} - 2\theta_{0,m}) D_m(\overline{\theta}) \mathrm{d}\overline{\theta} \quad [14a]$$

$$D_m(\theta_m) = K_m(\theta_m) \frac{\mathrm{d}h_m}{\mathrm{d}\theta_m} \quad [14b]$$

where $\overline{\theta}$ is a dummy variable. The diffusivity $D_m(\theta_m)$ can be easily computed from the hydraulic conductivity function

$K_m(\theta_m)$, and the derivative of the function $h_m(\theta_m)$ with respect to θ_m, written as $dh_m/d\theta_m$. The function $h_m(\theta_m)$ corresponds to the inverse function of the water retention function $\theta_m(h)$ defined by Eq. [2a]. More details on the use and validation of the model proposed by Haverkamp et al. (1994) can be found in Lassabatere et al. (2009).

Materials and Methods

Synthetic Data for Analytical Validation of BEST-2K

The synthetic DP soil is a loamy matrix with macropores, which corresponds to the loam texture defined in the soil catalog of Carsel and Parrish (1988). The hydraulic functions of this soil were described using the same equations as in BEST, i.e., the van Genuchten (1980) relationship with the Burdine (1953) condition for the water retention function and the Brooks and Corey (1964) relationship for the hydraulic conductivity. The fast-flow region corresponds to an ensemble of macropores of 1-mm average radius and occupies 10% of the bulk soil ($V_{tot,f}/V_{tot}$ = 0.1; Fig. 1). The scale parameter for water pressure head, $h_{g,f}$, was derived from the pore radius, $r_{g,f}$, using the Young–Laplace equation (Kutilek and Nielsen, 1994; Lenhard et al., 2005):

$$h_{g,f} = -\frac{\zeta}{r_{g,f}} \qquad [15a]$$

$$\zeta = \frac{2\sigma_{aw}\cos(\beta_c)}{\rho_w g} \qquad [15b]$$

where σ_{aw} is the surface tension of the air–water interface, β_c is the contact angle, ρ_w is the water density, and g is the gravitational acceleration constant, leading to a value of 14.9 mm^2 for ζ for the case of pure water. The value of the hydraulic conductivity, $K_{s,f}$, was computed from that of the loamy matrix, $K_{s,m}$, assuming a linear increase with the square of the pore radius, as indicated by Poiseuille's law (Sutera and Skalak, 1993) and suggested by several other studies (e.g., Watson and Luxmoore, 1986; Timlin et al., 1994). The residual water content, $\theta_{r,f}$, was set at zero and the saturated water content, $\theta_{s,f}$, at a large value of 0.70. The shape parameter, n_f, was set at 3.75 to induce a steep shape for the water retention functions, as commonly used for coarse soils (Schaap et al., 2001). Note that the matrix region and the bulk soil have ordinary porosities (approximately 43 and 45.7%, respectively), whereas the fast flow-region was assigned a high porosity (70%), assuming an ensemble of macropores surrounded by tiny walls made of few particles. In total, the fast-flow region occupies 10% of the bulk DP soil and its porosity constitutes 15.3% of the bulk porosity (i.e., $w_f\theta_{s,f}/\theta_{s,2K}$). The studied synthetic soil was designed to exhibit a typical DP behavior (see below).

Water infiltrations were analytically modeled using the analytical model developed by Lassabatere et al. (2014), where the three-dimensional, axisymmetric cumulative infiltration into DP soils was computed by the summation of the cumulative infiltration into each region multiplied by the volume fraction occupied by each region, and each cumulative infiltration was computed using the quasi-exact implicit model proposed by Haverkamp et al. (1994):

$$I_{3D,2K}(t) = w_f\left[I_{1D,f}(t) + \frac{\gamma_f S_f^2}{r_d\Delta\theta_f}t\right] + (1-w_f)\left[I_{1D,m}(t) + \frac{\gamma_m S_m^2}{r_d\Delta\theta_m}t\right] \qquad [16a]$$

$$\frac{2\Delta K_f^2}{S_f^2}t = \frac{1}{1-\beta_f}\left[\frac{2\Delta K_f}{S_f^2}\left[I_{1D,f}(t) - K_{0,f}t\right] - \ln\left(\frac{\exp\left\{\beta_f\frac{2\Delta K_f}{S_f^2}\left[I_{1D,f}(t) - K_{0,f}t\right]\right\} + \beta_f - 1}{\beta_f}\right)\right] \qquad [16b]$$

$$\frac{2\Delta K_m^2}{S_m^2}t = \frac{1}{1-\beta_m}\left[\frac{2\Delta K_m}{S_m^2}\left[I_{1D,m}(t) - K_{0,m}t\right] - \ln\left(\frac{\exp\left\{\beta_m\frac{2\Delta K_m}{S_m^2}\left[I_{1D,m}(t) - K_{0,m}t\right]\right\} + \beta_m - 1}{\beta_m}\right)\right] \qquad [16c]$$

where the subscripts m and f denote the parameters of the matrix and the fast-flow regions, respectively, and the variables r_d, $\Delta\theta$, ΔK, β, and γ are defined as in Eq. [13]. The sorptivity, S, of each region was computed with Eq. [14] using the initial and final water contents for each region.

We simulated a Beerkan experiment (zero water pressure head at the surface) and a TI experiment with a water pressure head fixed at −30 mm at the surface, which is twice the value of the scale parameter for water pressure head for the fast-flow region ($h_{g,f}$ = −14.9 mm) and should be enough to deactivate the fast-flow region during the TI experiment. Besides, this threshold is usually considered as a guide value for the hydraulic characterization of water infiltration with infiltrometers (Timlin et al., 1994). The water content at the end of the Beerkan experiment was equal to the bulk saturated water content, $\theta_{s,2K}$. For the TI experiment, the initial and final water contents, $\theta_{0,TI}$ and θ_{TI}, were computed from the local water retention functions using Eq. [1a], considering water pressure heads of −10 m and −30 mm, respectively. For the Beerkan experiment, the same initial water content was used. The cumulative infiltrations were computed for ideal conditions with a precise description of the transient state and attainment of the steady state. For the TI experiment, the cumulative infiltrations were computed in increments of 5 mm with a total cumulative infiltration of about 675 mm, and for the Beerkan experiment, the incremental and total cumulative infiltrations were about 0.15 and 40 mm, respectively. The total durations were 1500 and 10 min for the TI and Beerkan experiments, respectively.

To test the robustness of BEST-2K methods with respect to erroneous inputs, we simulated several scenarios. We inverted the analytical data using BEST-2K-A and BEST-2K-B and fixed the parameter w_f at several values other than the nominal value of 10%, specifically, 2, 4, 6, 7, 8, 9, 20, 30, and 40%. For the water contents, θ_{TI} was varied from 0.1 to 0.45 in steps of 0.01 for a nominal value of 0.405. The value of $\theta_{s,2K}$ was varied from 0.41 to 0.7 in steps of 0.01, for a nominal value of 0.457. For all these scenarios, the estimated hydraulic functions were compared with the estimates obtained with the nominal input values.

In the estimation of the shape parameters, we considered that the PTFs applied to the bulk PSD lead to the target values for shape parameters n_m and n_f. The bulk and local PSDs can be computed from the shape parameters N_m and N_f that correspond to the values of n_m and n_f with respect to the PTFs Eq. [t3–t6] in Table 1. In this analytical study, we did not question the accuracy of shape parameter estimates of BEST-2K and instead focused on the quality of the scale parameter estimates ($\theta_{r,m}$, $\theta_{s,m}$, $h_{g,m}$, $K_{s,m}$ and $\theta_{r,f}$, $\theta_{s,f}$, $h_{g,f}$, $K_{s,f}$), assuming that the shape parameters (n_m, η_m and n_f, η_f) are perfectly estimated. This aspect will be the subject of further studies.

Experimental Data for the Validation of BEST-2K

Three sites with different land uses were sampled for this investigation (Fig. 3). Two of these sites, located in northwestern Sardinia (Italy), were sampled in November 2017. The third site, located in a citrus orchard at the Department of Agriculture, Food and Forest Sciences of Palermo University (Italy), was sampled in July 2016. The soils are described according to the USDA soil classification system. The first Sardinia site (pasture; elevation of 20 m asl, near Alghero, about 6 km from the Mediterranean Sea) had a sandy clay loam soil. The second Sardinia site (agroforestry management; elevation of 333 m asl, near Villanova Monteleone in the province of Sassari) had a loam soil. This forest site had a low tree density (about 180 trees per hectare); the dominant tree species was the evergreen *Quercus suber* L. (cork oak), and forage species such as *Avena*, *Trifolium*, and *Lolium* grew under the trees. The Palermo University site (orchard; elevation of 38 m asl) had a sandy loam soil, and the trees were spaced in a 4- by 4-m grid.

For a given site, undisturbed soil cores (0.05 m in height and 0.05 m in diameter) were collected at 0- to 0.05- and 0.05- to 0.10-m depths and at three randomly selected points. Three disturbed soil samples (at 0–0.10-m depth) were also collected. The undisturbed soil cores were used to determine the dry soil bulk density, ρ_d, and the initial soil water content, θ_0, in the laboratory; the bulk saturated water content, $\theta_{s,2K}$, was determined from ρ_d (Eq. [5]). The disturbed soil was used to determine the PSD using conventional methods after H_2O_2 pretreatment to eliminate organic matter and clay deflocculation using sodium metaphosphate and mechanical agitation (Gee and Bauder, 1986). In particular, the fine size fractions were determined using the hydrometer method, and the coarse fractions were obtained by mechanical dry sieving. According to the USDA standards, three fractions, namely clay (0–2 μm), silt (2–50 μm), and sand (50–2000 μm), were also determined.

The cumulative infiltrations, $I_B(t)$ and $I_{TI}(t)$, as functions of time, t, were determined at zero water pressure head and a suction of 30 mm using the Beerkan method and an SW-080B infiltrometer. At each site, two Beerkan infiltration experiments were performed using a ring with an inner diameter of 0.15 m inserted to a depth of about 0.01 m to avoid lateral loss of the ponded water, as recommended by Lassabatere et al. (2006). A known volume of water (150 mL) was poured into the cylinder, and the elapsed

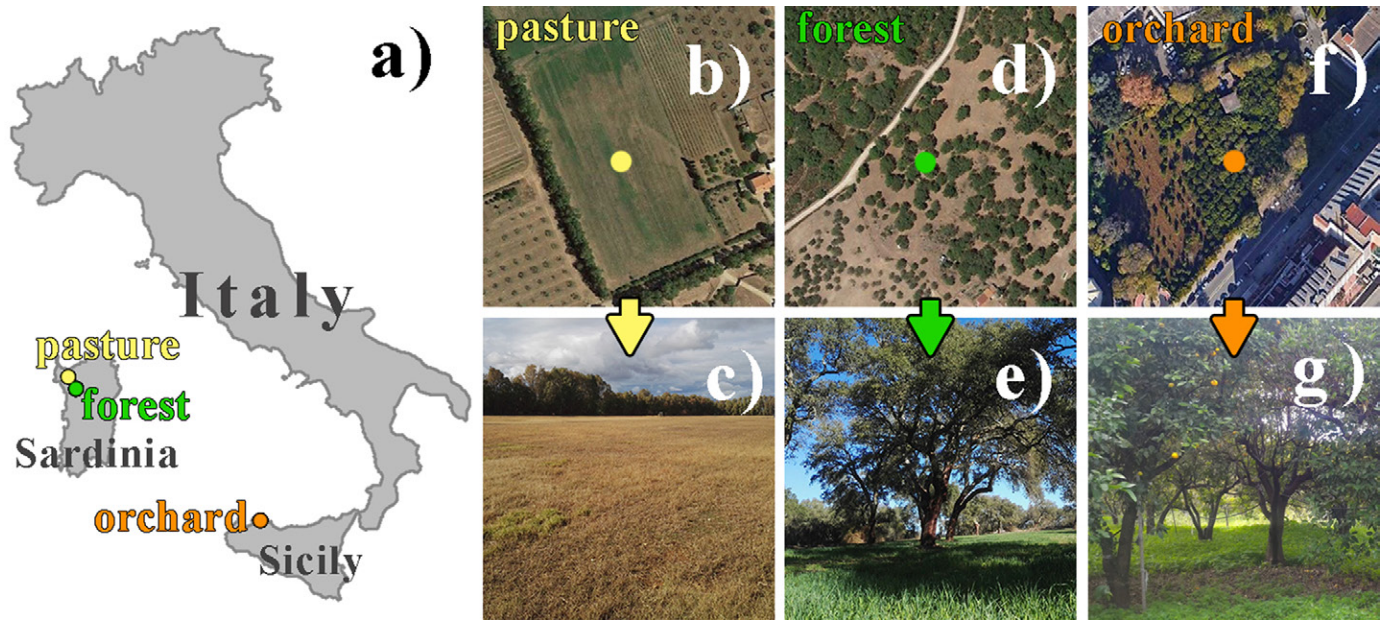

Fig. 3. Experimental sites: (a) locations of the study areas in Italy; and (b,c) pasture, (d,e) forest, and (f,g) orchard sites.

time during the infiltration was measured. When the water had completely infiltrated, the same amount of water was poured into the cylinder again, and the time needed for the water to completely infiltrate was measured once more. This process was repeated until the difference in infiltration times between three consecutive water supplies was negligible; this indicated that a practically steady infiltration rate had been achieved. An SW-080B infiltrometer with a 0.20-m-diameter porous plate was applied close to each Beerkan experiment. The intermediate volumetric water content, θ_{TI}, was determined on a small amount of soil sampled under the porous plate at the end of the water infiltration experiment.

Each site was characterized by single ρ_d, θ_0, $\theta_{s,2K}$, θ_{TI}, and PSD data obtained by averaging the individual measurements, except for the orchard site where specific measurements were performed similar in manner to the TI and Beerkan experiments at two different locations. The experimental infiltration data were inverted using the BEST-2K-A method along with three methods: Slope, Intercept, and Steady for BEST-1K. For the BEST-2K-A method, without additional information, w_f was estimated as the arithmetic mean of the constraints defined by Eq. [9].

BEST-1K Methods

The BEST methods are synthesized in Table 1, using equations that begin with the letter *t*. As described above, these methods use the van Genuchten (1980) relation with Burdine condition for the water retention function, $h(\theta)$, and the Brooks and Corey (1964) model for hydraulic conductivity, $K(\theta)$ (Table 1, Eq. [t1]). The assumptions of the BEST methods are described next. The value of θ_r is assumed to be zero, and the saturated water content θ_s equals the soil porosity, which is computed by Eq. [t1d]. The shape parameters n and η are estimated from the PTFs that use the PSD of the size fraction <2 mm (Table 1). The PSD is fitted to Eq. [t2] (Table 1), which is consistent with the water retention function (Table 1, Eq. [t1a]), and the related shape parameters, M and N, are inserted in the PTFs (Table 1, Eq. [t3–t7]). Then the scale parameters, K_s and h_g, are derived from the analysis of the cumulative infiltrations. Three BEST methods were developed, including the original method (BEST Slope; Lassabatere et al., 2006), a method dedicated to coarse media (BEST Intercept; Yilmaz et al., 2010), and another relying only on steady state (Bagarello et al., 2014). These three methods use the same analytical model to fit the experimental data, which includes two approximate expansions for the transient and steady states (BEST analytical models, Table 1). These expansions were developed to approximate the quasi-exact implicit formulation proposed by Haverkamp et al. (1994) and were validated numerically by Lassabatere et al. (2009). The three methods differ in how they perform the fit (BEST fitting algorithm for cumulative infiltration, Table 1). BEST Slope uses the first part of the cumulative infiltration curve to fit the transient state expansion (Table 1, Eq. [t16]) and the slope of the final part to describe steady state (Table 1, Eq. [t14]). BEST Intercept uses the first part of the cumulative infiltration to fit to the same transient expansion (Table 1, Eq. [t17]) but uses the intercept of the steady-state straight line described by the final points (Table 1, Eq. [t14]). Finally, BEST Steady makes use of only the steady-state straight line and its slope and intercept (Table 1, Eq. [t14]). The saturated soil hydraulic conductivity, K_s, and sorptivity, S, are then derived from these fitting procedures (Table 1, Eq. [t15–t19]). The scale parameter for the water retention function, h_g, is derived from these previous estimates (Table 1, Eq. [t20]). Thus, all unsaturated hydraulic parameters are estimated, and the complete water retention and hydraulic conductivity functions can be determined.

In comparison to the application of BEST methods for SP soils in the field, the use of BEST-1K methods within the framework of BEST-2K differs in the quantification of the inputs. The bulk saturated water content, $\theta_{s,2K}$, is still defined using the bulk density. However, the local saturated water contents $\theta_{s,m}$ and $\theta_{s,f}$ are computed from $\theta_{s,2K}$ and θ_{TI} using the BEST-2K preprocessing functions. In the BEST-2K framework, BEST-1K no longer fits the bulk PSD to the unimodal model of Eq. [t2] (Table 1). Instead, the bulk PSD is fitted to a bimodal model (Eq. [3]) to derive the PSD shape parameters N_m, M_m, N_f, and M_f to be used in the BEST-1K PTFs (Eq. [t3–t7]) for the derivation of the shape parameters n_m, η_m, n_f, and η_f. Last, the initial water contents ($\theta_{0,m}$, $\theta_{0,f}$) and the Beerkan cumulative infiltration ($I_{B,m}$, $I_{B,f}$), which are needed for the application of the BEST-1K fitting functions, are provided by BEST-2K preprocessing functions from the bulk measurements (θ_0, θ_{TI}, I_{TI}, I_B). More details are provided with the illustration of the treatment of one dataset in the supplemental material.

Results

Validation of BEST-2K with Synthetic Data

Synthetic Experimental Data

Before presenting the application of BEST-2K, we present the analytical data (hydraulic curves, water contents, and cumulative infiltrations) for the synthetic soil. The synthetic soil exhibits the water retention and hydraulic conductivity functions that show the effect of the fast-flow region (Fig. 4a and 4b). This region induces a steep increase in water content and hydraulic conductivity close to saturation; in particular, the hydraulic conductivity increases by two orders of magnitude (Fig. 4b). This increase draws an inflection point on the plots of the water retention and hydraulic conductivity functions (Fig. 4a and 4b, A) that marks the transition between the activation of the matrix alone and the concomitant activations of the matrix and fast-flow regions. This graphical pattern is typical in DP systems (Durner, 1994) and must be considered as one of the crucial points for assessing the accuracy of BEST-2K.

The occurrences of flow in both the matrix and fast-flow regions impact the soil response to hydraulic solicitations. The water content measured at the end of the TI experiment is less than the bulk saturated content due to the deactivation of the fast-flow region, which leads to $\theta_{TI} < \theta_{s,2K}$ (Fig. 4c, DP). Instead, the water content would have remained constant for SP soils composed of only the matrix, i.e., $\theta_{TI} \approx \theta_{s,m}$ (Fig. 4c, SP). However,

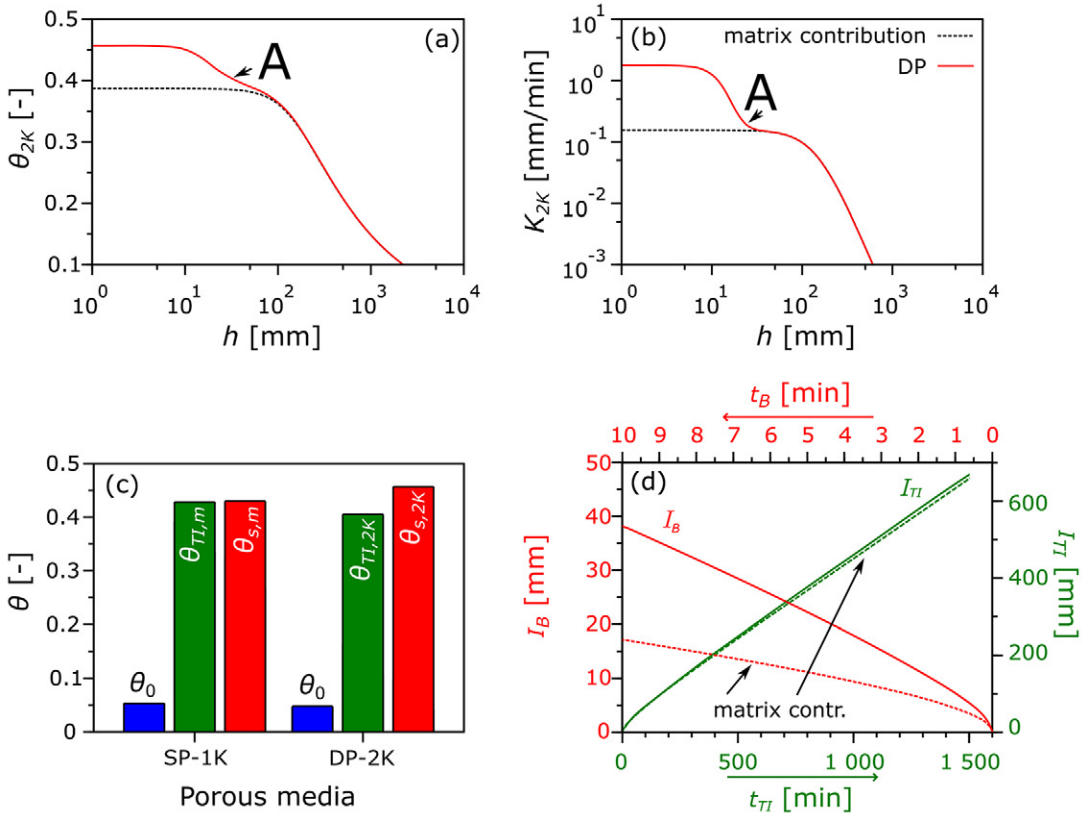

Fig. 4. Hydraulic characteristic curves: (a) water retention and (b) hydraulic conductivity of the synthetic dual-permeability (DP) soil; (c) water contents at time zero (θ_0) and at the end of the tension infiltrometer (TI) experiment (θ_{TI}), and bulk saturated water content (θ_s) for the single-permeability (SP) soil (matrix alone, SP-1K) and the DP soil (DP-2K), (d) cumulative infiltration into the synthetic DP soil for the TI experiment (I_{TI}) and for the Beerkan experiment (I_B) with the contribution of the matrix (matrix contr.). The letter A refers to comments in the text.

the difference in the water content remains within the range of 5% for DP soils. These results show that comparison of water contents measured after the TI experiments with the soil porosity could help in detecting the occurrence of DP behavior, provided that the measurement uncertainty is low enough (on the order of 1%).

Regarding the cumulative infiltration curves, the contribution of the fast-flow region to the total cumulative infiltration is minimal for the TI experiment, with an alignment of the matrix contribution to the bulk cumulative infiltration (Fig. 4d, I_{TI}). Conversely, for the Beerkan experiment, the fast-flow region has a large contribution to the bulk cumulative infiltration (Fig. 4d, I_B). Thus, the fast-flow region contributes more to cumulative infiltration in the Beerkan experiments than in the TI experiments. Large differences in cumulative infiltration between the TI and Beerkan experiments could indicate the occurrence of DP behavior.

Application of BEST-2K Methods to Synthetic Data

A full description of the application of the BEST-2K method to the analytical data is presented in the supplemental material. For clarity and parsimony, we focus on the discussion of the BEST-2K results and their accuracy. One observation is that the three BEST-1K methods (BEST Slope, Intercept, or Steady) lead to similar results and estimates. The application of the two BEST-2K methods, BEST-2K-A and BEST-2K-B, to error-free analytical data provided sets of hydraulic parameters quite similar to each other, leading to close water retention and hydraulic conductivity functions. Given the similarity of the results, we illustrate only the results for the case of BEST-2K-A coupled with the BEST Slope method of BEST-1K.

The estimated functions are nearly identical to the targets (Fig. 5a and 5b); in particular, the estimated hydraulic parameters are on the same order of magnitude as the target parameters listed in Table 2 (columns Target for the target and (1) for BEST-2K-A). However, the accuracy of BEST-2K can be improved. The shapes and, in particular, the bimodality of the target water retention and hydraulic conductivity functions are not properly depicted because the inflection point of the target functions is more conspicuous (Fig. 5a and 5b). The analysis of the hydraulic parameters shows that the saturated water contents and hydraulic conductivities are properly estimated, with relative errors <10 to 20%, except for the scale parameter $h_{g,f}$ with relative errors around 110% (Table 2). In fact, the scale parameter for water pressure head $|h_g|$ is slightly underestimated for the matrix and largely overestimated for the fast-flow region. As a result, the difference in $|h_g|$ between the matrix and fast-flow regions decreases. This means that when the water pressure head increases from $h_{g,m}$ to $h_{g,f}$, the smallest pores of the fast-flow

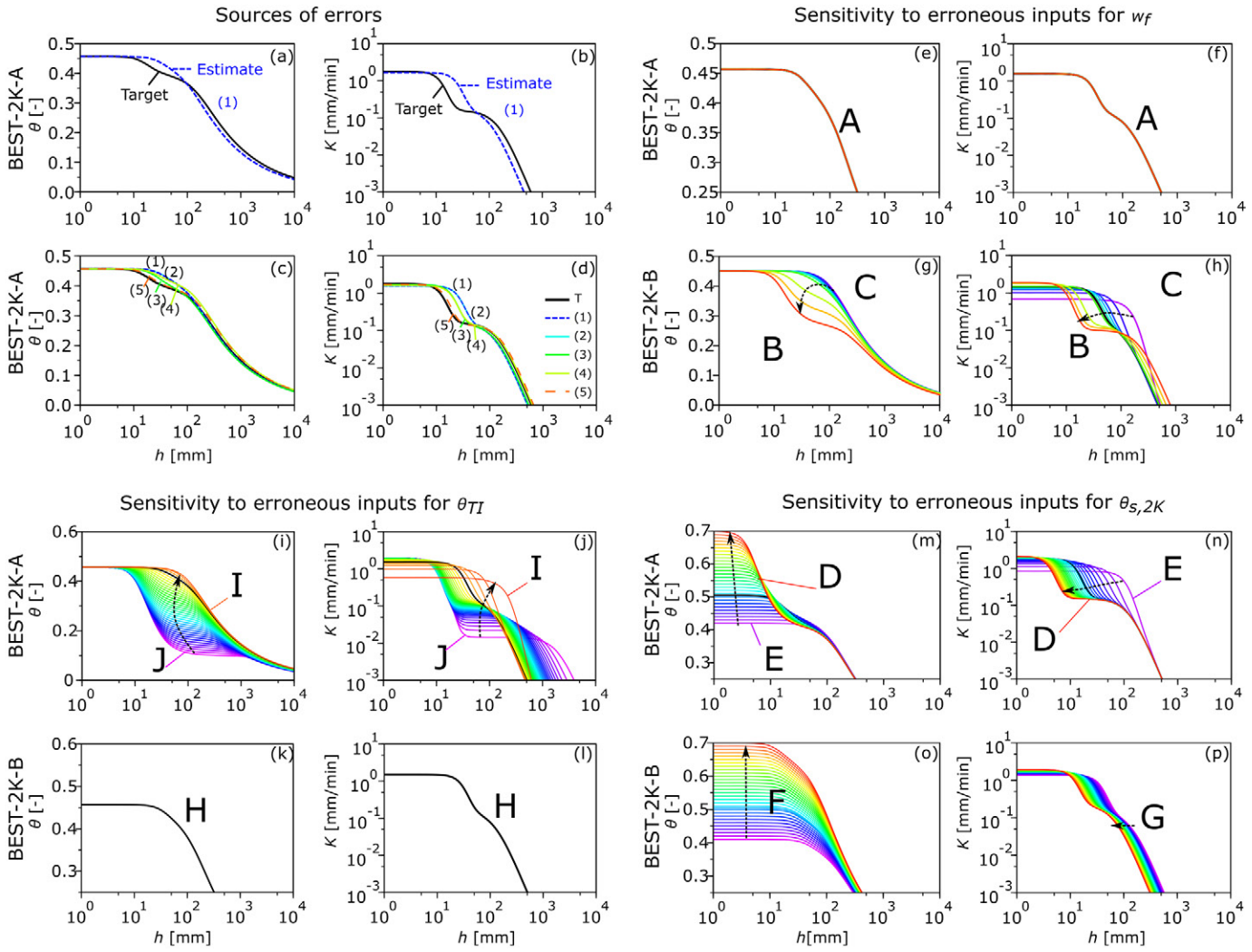

Fig. 5. Impacts of BEST-2K preprocessing functions on BEST-2K accuracy: (a–d) analysis of the sources of errors for BEST-2K-A by comparison of the target curves (T) with those estimated by BEST-2K-A (1), of BEST-2K-A without errors related to the computation of initial water contents (2), saturated water content (3), cumulative infiltrations (4), and without any error related to inputs (5); and influence of input accuracy on BEST-2K estimates for (e–h) errors in estimation of parameter w_f, (i–l) erroneous inputs for the measured water content after the tension infiltrometer (TI) experiment θ_{TI}, and (m–p) erroneous inputs for the bulk saturated water content $\theta_{s,2K}$. The large uppercase letters refer to comments in the text. The arrows show the direction of change of the estimated hydraulic functions when the parameter is increased. The black lines refer to the hydraulic functions estimated by BEST-2K.

region begin to fill with water before the largest pores of the matrix. In other words, the more the activation of the matrix and fast-flow regions overlap, as well as their contributions to the bulk hydraulic conductivity, the less evident is the bimodality. Thus, the BEST-2K methods underestimate the contrast between the matrix and fast-flow regions, i.e., the magnitude of the DP behavior is underestimated.

Analysis of Sources of Errors

The discrepancy between the target and estimated functions results from the errors that may be induced either by the BEST-2K preprocessing functions that provide input to BEST-1K or by the application of BEST-1K itself. Here, we assess the errors due to the preprocessing functions by comparing the target function and related parameters to those obtained with BEST-2K based on the following scenarios:

1. All preprocessing function errors, i.e., the errors due to the computation of the initial water content ($Er\theta_0$), saturated water content ($Er\theta_s$), and cumulative infiltrations ($Er\mathit{I}$)
2. Similar to (1) but without the error $Er\theta_0$
3. Similar to (1) but without the error $Er\theta_s$
4. Similar to (1) but without the error $Er\mathit{I}$
5. The version with residual errors due to the application of BEST-1K.

To perform this assessment, we replaced the inputs provided by the preprocessing functions, ($\theta_{0,m}$, $\theta_{s,m}$, $I_{B,m}$ and $\theta_{0,f}$, $\theta_{s,f}$, $I_{B,f}$), by the real values before processing them with BEST-1K (Fig. 2). The real values were directly computed from the synthetic hydraulic functions (Eq. [1]) for water contents and the analytical models (Eq. [16b] and [16c]) for the cumulative infiltrations. The removal of $Er\theta_0$ does not significantly improve the estimates

(Table 2, Scenario 2, Fig. 5c and 5d). However, the removal of Erθ_s or ErI (Table 2, Scenario 3 or 4, respectively) leads to a significant improvement. Very accurate estimates are obtained when all errors are removed, with residual relative errors mostly below 10% (Table 2, Scenario 5) and a good agreement between the estimated and target functions (Fig. 5c and 5d). In conclusion, the errors produced by the preprocessing functions, and in particular Erθ_s and ErI, explains most of the discrepancy between the target and BEST-2K estimates. In addition, the residual error due to BEST-1K can be considered negligible in this particular case. Note that for these results, as stated above, the shape parameters n_m and n_f are assumed to be perfectly estimated, although these may involve a supplementary source of error. The investigation of the impact of erroneous estimations of shape parameters on the accuracy of BEST-2K will be the subject of further studies.

In the previous results, the experimental inputs (PSD, θ_0, θ_{TI}, $\theta_{s,2K}$, I_{TI}, and I_B) were considered error free, and parameter w_f (the volume fraction occupied by the fast-flow region) was perfectly known. Here, we first assess the robustness of BEST-2K-A and BEST-2K-B with regard to erroneous estimations of w_f, which is a key parameter for the BEST-2K preprocessing functions and one that is also complicated to estimate (Kodešová et al., 2010). In addition, we investigate the robustness of these methods with regard to erroneous inputs of θ_{TI} and $\theta_{s,2K}$. Indeed, the measurement of water contents in the field is known to be subject to uncertainties in the soil moisture probe, which renders the estimation θ_{TI} difficult. Besides, the measure of bulk density that is needed for the determination of $\theta_{s,2K}$ may also be subject to uncertainty. However, θ_{TI} and $\theta_{s,2K}$, and the difference between them, are key parameters of the BEST-2K preprocessing functions. Last, the quality of cumulative infiltrations I_{TI} and I_B impacts the quality of the cumulative infiltrations $I_{B,f}$ and $I_{B,m}$, which in turn impacts the degree of success of the treatment with BEST-1K. This is particularly true for the BEST Slope and BEST Intercept methods, which need a proper description of both the transient and steady states. In this case, the problem is not with the BEST-2K approach but with the efficiency with which the BEST-1K methods handle imprecise descriptions of the cumulative infiltrations. This issue is addressed below with a discussion of the field experimental data.

Sensitivity of BEST-2K Methods to Erroneous Estimates of the Volume Ratio Occupied by the Fast-Flow Region

The parameter w_f is used in most of the parts of the BEST-2K methods, including all the preprocessing functions for computing the inputs $\theta_{0,m}$, $\theta_{s,m}$, $I_{B,m}$ and $\theta_{0,f}$, $\theta_{s,f}$, $I_{B,f}$, and the water retention and hydraulic conductivity functions used for computing $\theta_{2K}(h)$ and $K_{2K}(\theta)$ (Fig. 2). Despite its potentially significant influence, w_f does not impact the water retention and hydraulic conductivity functions predicted by BEST-2K-A (Fig. 5e and 5f, A). In fact, the values of the hydraulic parameters vary with w_f, yet they produce similar hydraulic functions. However, for BEST-2K-B, w_f has a strong influence on the predicted water retention and hydraulic conductivity functions (Fig. 5g and 5h). An increase in w_f increases the bulk saturated hydraulic conductivity $K_{s,2K}$ and the contrast

Table 2. Impact of preprocessing functions on the accuracy of BEST-2K-A: target hydraulic parameters corresponding to the synthetic soil (Target), BEST-2K-A estimates (1), and BEST-2K-A estimates without errors in the computation of initial water content (2), final water contents (3), cumulative infiltration (4), and without any errors on the computation of BEST-1K inputs (5).

Parameter†	Target	(1) Erθ_0 + Erθ_s + ErI	(2) Erθ_s + ErI	(3) Erθ_0 + ErI	(4) Erθ_0 + Erθ_s	(5) Residual errors
			Matrix			
$\theta_{s,m}$	0.430	0.450	0.450	0.430	0.450	0.430
$\lvert h_{g,m}\rvert$, mm	144.0	122.6	122.6	131.1	151.2	161.8
$K_{s,m}$, mm min^{-1}	1.73×10^{-1}	1.67×10^{-1}	1.67×10^{-1}	1.60×10^{-1}	1.68×10^{-1}	1.60×10^{-1}
			Matrix error, %			
$\theta_{s,m}$	–	4.8	4.8	0.0	4.8	0.0
$\lvert h_{g,m}\rvert$	–	14.9	14.9	9.0	5.0	12.3
$K_{s,m}$	–	3.9	3.9	8.0	3.2	7.6
			Fast-flow region			
$\theta_{s,f}$	0.700	0.516	0.516	0.700	0.516	0.700
$\lvert h_{g,f}\rvert$, mm	14.9	31.3	31.3	23.5	23.6	16.9
$K_{s,f}$, mm min^{-1}	1.62×10^{1}	1.42×10^{1}	1.42×10^{1}	1.55×10^{1}	1.46×10^{1}	1.58×10^{1}
			Fast-flow region error, %			
$\theta_{s,f}$	–	26.3	26.3	0.0	26.3	0.0
$\lvert h_{g,f}\rvert$	–	109.8	109.8	57.8	58.2	13.7
$K_{s,f}$	–	12.6	12.6	4.6	10.1	2.6

† θ_s, saturated water content; $\lvert h_g\rvert$, scale parameter for water pressure head; K_s saturated hydraulic conductivity. The matrix and fast-flow regions are indicated by subscripts *m* and *f*, respectively.

in parameter h_g between the matrix and fast-flow regions, which leads to a very conspicuous inflection point and bimodal shape of the water retention and hydraulic conductivity functions (Fig. 5g and 5h, B). However, when the value of w_f is too small, the estimated hydraulic functions tend toward unimodal curves, which correspond to SP soils (Fig. 5g and 5h, C). These results show that the BEST-2K-B method is very sensitive to the prior estimation of the volume ratio w_f, in contrast to BEST-2K-A. Therefore, BEST-2K-A should be used when the volume ratio w_f cannot be estimated properly. Another finding is that BEST-2K-A and BEST-2K-B provided accurate fits for the cumulative infiltrations for all scenarios. There was no degradation of fits when parameter w_f was varied from its nominal value. Consequently, the quality of fits cannot be used to identify parameter w_f. In general terms, parameter optimization may be problematic when many parameters are considered (Angulo-Jaramillo et al., 2016). With reference to the results obtained here, additional data are needed to properly estimate parameter w_f prior to running the BEST-2K methods because this parameter cannot be estimated by fitting the cumulative infiltration data.

Sensitivity of BEST-2K Methods to Erroneous Inputs for the Bulk Saturated Water Contents

For the BEST-2K-A method, erroneous values of $\theta_{s,2K}$ impact only the computation of the saturated water content for the fast-flow region $\theta_{s,f}$. Inputs θ_{0m}, $\theta_{s,m}$, and $I_{B,m}$ remain unchanged (see Eq. [4a], [7b], and [12a]), leading to similar hydraulic parameters for the matrix. However, the changes are drastic for the fast-flow region. When $\theta_{s,2K}$ is overestimated, the bulk hydraulic functions exhibit an increase in saturated water content $\theta_{s,2K}$ and saturated hydraulic conductivity $K_{s,2K}$ along with a more conspicuous bimodality (Fig. 5m and 5n, D). On the other hand, when $\theta_{s,2K}$ is underestimated, the hydraulic functions tend toward unimodal curves (Fig. 5m and 5n, E). For the BEST-2K-B method, erroneous determinations of $\theta_{s,2K}$ directly impact the estimates of saturated water contents for both the matrix and fast-flow regions, $\theta_{s,m}$ and $\theta_{s,f}$, which in turn affects the estimates of the other hydraulic parameters. When $\theta_{s,2K}$ is increased, the bulk saturated water content and saturated hydraulic conductivity increase, whereas the scale parameter $|h_g|$ decreases. Consequently, water retention functions move upward (Fig. 5o, F) and hydraulic conductivity functions move toward the left (Fig. 5p, G), which indicates more permeable soils with less capillarity. The bimodality of the curves remains similar across the range of $\theta_{s,2K}$ values (Fig. 5o and 5p, G). The BEST-2K-B method was found to be more sensitive for the estimation of the water retention function than for the hydraulic conductivity function (Fig. 5o vs. 5p). In terms of bimodality of the hydraulic conductivity function, BEST-2K-B is less sensitive to the accuracy of $\theta_{s,2K}$ than BEST-2K-A.

Sensitivity of BEST-2K Methods to Erroneous Inputs for Tension Infiltrometer Water Contents

BEST-2K-B does not use θ_{TI} and is therefore entirely insensitive to this parameter (Fig. 5k and 5l, H). For BEST-2K-A, an erroneous input for θ_{TI} induces errors in the estimates of the saturated water content for both the matrix and fast-flow regions, which in turn impacts the estimates of the other hydraulic parameters. When θ_{TI} increases, the parameter $|h_g|$ increases for the fast-flow region, thus approaching that of the matrix region. As a result, unimodal curves are obtained (Fig. 5i and 5j, I). For underestimated values of θ_{TI}, the fast-flow region is predicted as being too dominant, which leads to extremely bimodal hydraulic functions and a complete separation of the fast-flow and matrix regions (Fig. 5i and 5j, J). In such a case, the estimated hydraulic functions differ significantly from the target functions. Clearly, particular attention must be paid to the accuracy of the input parameter θ_{TI} when using BEST-2K-A.

The main conclusion of the sensitivity analysis is that, provided the measurement uncertainty does not undermine the quality of the BEST-2K inputs, either BEST-2K-A or BEST-2K-B may be used. In addition, the estimated hydraulic functions are not significantly different from the target functions. These results validate the BEST-2K approach numerically. However, because BEST-2K-B is very sensitive to the prior estimation of w_f, this method should not be used when the estimation of w_f is uncertain. On the other hand, the main advantage of BEST-2K-B over BEST-2K-A is that BEST-2K-B does not require the measurement of water contents at the end of the TI experiments, whereas the quality of the water content measurement significantly influences the quality of estimates obtained using BEST-2K-A. BEST-2K-B is preferable when there are large uncertainties in the water content measurements.

Finally, it should be noted that although BEST-2K-A and BEST-2K-B use the initial water content θ_0, the experiments performed with this input are not presented because uncertainty in θ_0 has no impact on the results. Furthermore, θ_{TI} and $\theta_{s,2K}$ are not subject to the same uncertainties in the field. Indeed, in contrast to θ_{TI}, $\theta_{s,2K}$ is not directly measured but rather is inferred from the measurement of bulk density, which is probably subject to less uncertainty. Nevertheless, the value of $\theta_{s,2K}$ must be precise because it affects the BEST-2K-A and BEST-2K-B methods.

Application of BEST-2K Method to Real Data

Experimental Results

The experimental data that were collected for the three sites are depicted in Fig. 6, and the physical parameters are listed in Table 3. The bulk saturated water content $\theta_{s,2K}$ has high values for the forest and orchard sites and lower values for the pasture site (Table 3). The volumetric water contents θ_{TI} are significantly lower than the saturated water contents, except for the pasture site. The cumulative infiltrations vary with the site, with much larger infiltrations for the orchard site and comparable infiltrations for the forest and pasture sites (Fig. 6b and 6d). This difference may be due to the soil texture and structure, with finer soils at the forest and pasture sites and a coarse texture and more open structure at the orchard site. The cumulative infiltrations obtained with the Beerkan method are much higher than those obtained with the

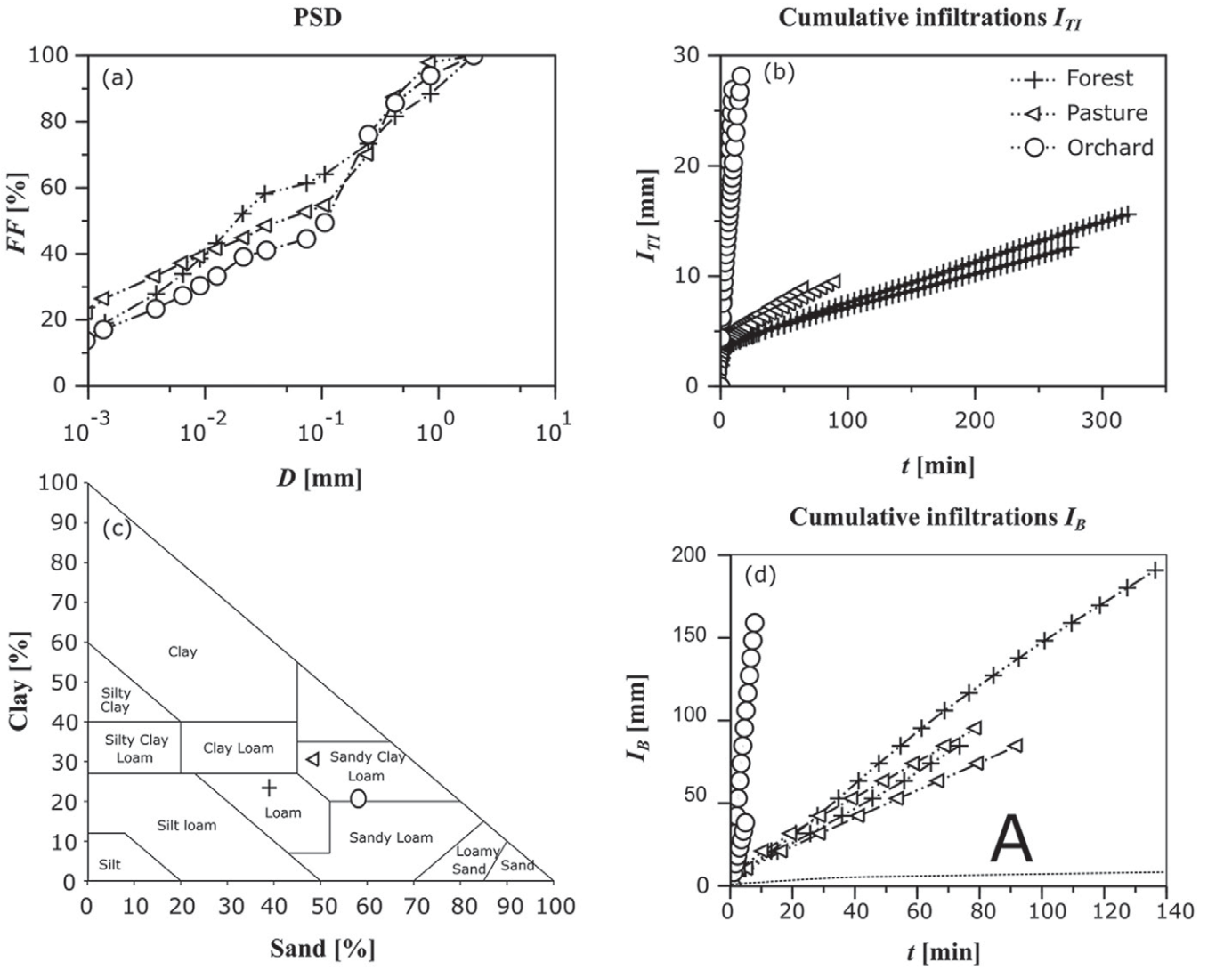

Fig. 6. Experimental data collected for three soils: (a) particle size distributions (PSD); (b) cumulative infiltration obtained with the tension infiltrometer (I_{TI}); (c) textural triangle and textural properties; (d) cumulative infiltration obtained for the Beerkan experiments (I_B), with the cumulative infiltration for the tension infiltrometer represented with dashed lines for the orchard soil (A).

TI (Fig. 6d, A), which indicates a potential for DP behavior for the three soils (Gonzalez-Sosa et al., 2010); the large increase corresponds to the activation of the macropore network in these soils (Lassabatere et al., 2014).

Illustration of the Case of Orchard 2 (Orchard Site)

For the analysis of these experimental data, we considered only BEST-2K-A, since the volume fraction occupied by the fast-flow region is not known a priori and erroneous estimations of this parameter may undermine the quality of BEST-2K-B estimates. However, as discussed above, the BEST-2K-A method requires a very accurate measure of the water content θ_{TI}. In addition, if BEST-2K-A is able to match the target hydraulic functions with any value of the parameter w_f, the estimates for hydraulic parameters may still be erroneous for erroneous values of w_f (see above).

BEST-2K-A was successfully applied to all the trials, and it provided accurate fits and plausible estimates for most of the hydraulic parameters. As an example, Fig. 7a to 7h illustrate some key findings for the specific case of the Orchard 2 trial. First, the bimodal model for the PSD is more accurate than the unimodal model (Fig. 7a vs. 7b), with a more precise modeling of intermediate points and the two modes around 10 and 10^3 μm (Fig. 7a, A). Second, the fit of the model to the experimental infiltration curves was also accurate (Fig. 7c–7f). For the matrix region, the transient-state model was adjusted based on the complete dataset (Fig. 7c and 7d, B) because the transient state was longer than the total duration of the experiments. This result points to the difficulty in reaching steady state, which indicates potential estimation errors in the BEST-1K methods (i.e., Slope, Intercept, and Steady) that require the attainment of a steady state. In contrast, for the fast-flow region, the transient state was extremely short and the steady state was attained in a very short time (Fig. 7e and 7f). The transient state is represented by two points only, including the starting point ($t_B = 0, I_{B,f} = 0$) (Fig. 7f, C), whereas the steady-state model

matches most of the dataset (Fig. 7e, D). This pattern probably impacts the quality of BEST-1K and thus the accuracy of estimations for the fast-flow region (e.g., Di Prima et al., 2016). In addition, this pattern was often encountered, which highlights the necessity of having a precise description of the transient state at very short times for the Beerkan test. After the completion of the infiltration experiments, the bulk hydraulic parameters and hydraulic functions were characterized (Fig. 7g and 7h). The estimated hydraulic functions clearly show the activation of the fast-flow region close to saturation, with an increase in both the water content and hydraulic conductivity. The graphs show that the bimodality of the hydraulic conductivity curve is much more pronounced than that of the water retention curve (Fig. 7h, E).

Water Retention and Hydraulic Conductivity Functions for the Three Sites

The water retention and hydraulic conductivity functions estimated for the three sites are depicted in Fig. 7i to 7p. The comparison of the sites shows that the forest and orchard sites have the highest values of saturated water content (Fig. 7i, F) and hydraulic conductivity (Fig. 7j, G). The same hydraulic functions are shown in Fig. 7k to 7p with the contribution of the matrix region for each site. For the two tests performed at the forest site, the bulk hydraulic conductivity functions align with the matrix contribution until an inflection point (Fig. 7l, H), after which the bulk hydraulic functions deviate due to the contribution of the fast-flow region. A similar pattern is obtained for Orchard 2, as depicted in Fig. 7o and 7p (M). The inflection points and shifts in the curves reveal the effect of the activation of the fast-flow region in boosting the bulk water retention and hydraulic conductivity functions. For these cases, the BEST-2K method predicts a clear DP behavior with a higher value of $|h_g|$ for the matrix region in comparison to the fast-flow region (Table 4, Forest 1, Forest 2, and Orchard 2). In contrast, for Orchard 1, the bulk water retention and hydraulic conductivity functions are unimodal without any inflection point (Fig. 7p, L). Similar but more pronounced trends are shown for the pasture site (Fig. 7m and 7n, J and K). In these cases, BEST-2K predicts values of $|h_g|$ that are much larger for the fast-flow region (Table 4, Orchard 1, Pasture 1, and Pasture 2), which is not physically realistic. Indeed, larger values of $|h_g|$ are associated with soils that have smaller pore sizes and thus can increase water retention by capillarity (Angulo-Jaramillo et al., 2016).

Table 3. Coordinates, clay, silt, and sand content (USDA classification system) in the 0- to 10-cm depth range, soil textural classification, dry soil bulk density (ρ_d), initial volumetric soil water content (θ_0), bulk saturated volumetric water content ($\theta_{s,2K}$), and volumetric water content obtained at −30 mm (θ_{TI}) for the sampled soils at the pasture (Alghero), forest (Villanova Monteleone), and orchard (Palermo) sites.

Variable	Pasture	Forest	Orchard
Coordinates	40°37′33.7″ N, 8°21′0.4″ E	40°27′5.0″ N, 8°30′47.5″ E	38°6′25.7″ N, 13°21′7.7″ E
Clay, %	29.0 (0.39)†	22.2 (0.70)	21.0 (2.02)
Silt, %	21.6 (2.17)	37.6 (1.00)	23.8 (3.72)
Sand, %	49.4 (2.19)	40.2 (1.06)	54.3 (3.67)
Textural classification	sandy clay loam	loam	sandy loam
ρ_d, g cm^{-3}	1.640 (0.08)	0.842 (0.04)	1.085 (0.08)
θ_0, cm^3 cm^{-3}	0.244 (0.02)	0.300 (0.08)	0.110 (0.05)
$\theta_{s,2K}$, cm^3 cm^{-3}	0.381 (0.03)	0.603 (0.02)	0.584 (0.02)
θ_{TI}, cm^3 cm^{-3}	0.347 (0.05)	0.312 (0.01)	0.323 (0.02)

† Standard deviations are indicated in parentheses.

Several hypotheses may be evoked for the difficulty in characterizing half of the trials. First, these trials may not involve any fast-flow region or preferential flow. Specific investigations are needed to examine what happens when BEST-2K is applied to SP soils. Besides, the difficulty in estimating the hydraulic functions and parameters may explain a part of the failure. As discussed above, proper estimation of h_g for the matrix region requires a steady-state water infiltration condition, which may take too long to attain. On the other hand, the opposite conditions create difficulties in estimating the parameter h_g for the fast-flow region. Like most permeable porous media with small sorptivity, the transient states are very short, which gives too little time to properly sample the transient state and leads to errors in estimating the parameter h_g. In addition, the estimation of the volume fraction occupied by the fast-flow region, w_f, remains problematic, with potential impacts on the estimation of the hydraulic parameters. However, despite these shortcomings, the prospects of applying the BEST-2K methods to real experimental data are quite promising. Indeed, BEST-2K provided good fits with plausible results for several trials performed in this study. In half of the cases, the methods were able to characterize the bimodality of the water retention and hydraulic conductivity functions.

Comparison of BEST-2K and BEST-1K

BEST-1K methods were also used to retrieve water retention and hydraulic conductivity functions corresponding to SP soils considering the inputs PSD, θ_0, $\theta_{s,2K}$, and I_B. The fit of the PSD had to be restricted to the first mode, which gave similar results. In all cases, good fits were obtained for the cumulative infiltration I_B. However, the derived hydraulic parameters and related water retention and hydraulic conductivity curves corresponded to different hydraulic parameters and hydraulic functions. These estimated water retention and hydraulic conductivity curves were used to compute the cumulative infiltration corresponding to an imposed water head of −30 mm and to enable a comparison with the experimental data I_{TI}. The cumulative infiltrations corresponding to the BEST-1K hydraulic parameters were also compared with those obtained with BEST-2K. For the soils that are predicted by BEST-2K to have a clear DP behavior (bimodality of the water retention and hydraulic conductivity curves), the TI cumulative infiltrations predicted by BEST-1K were less accurate than those predicted by BEST-2K. This is particularly the case for Orchard 2. For this case, BEST-1K predicts a very permeable and draining behavior, typical of coarse soil with very little water retention by capillarity. At −30 mm, many pores are already deactivated and do

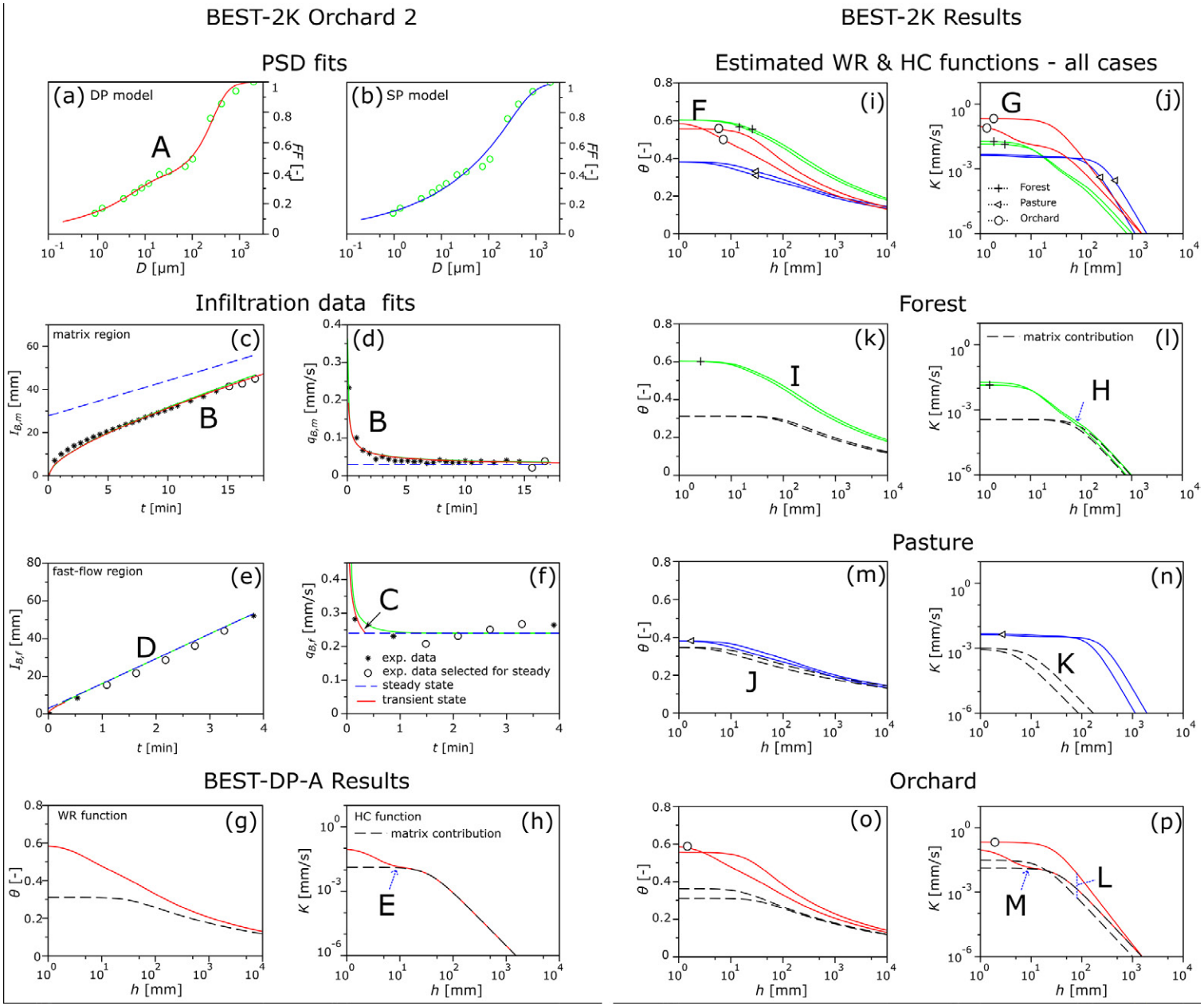

Fig. 7. (a–h) Application of BEST-2K-A to the Orchard 2 soil: PSD fitted with (a) the bimodal and (b) the unimodal models, (c,d) fit of Beerkan cumulative infiltration into the matrix $I_{B,m}$ and related infiltration rate $q_{B,m}$, (e,f) fit of Beerkan cumulative infiltration into the fast-flow domain $I_{B,f}$ and related infiltration rate $q_{B,f}$, and (g,h) estimated water retention (WR) and hydraulic conductivity (HC) functions; (i–p) BEST-2K-A results for all cases, with details for the (k,l) forest, (m,n) pasture, and (o,p) orchard sites. The uppercase letters refer to comments in the text; the dashed lines represent the contribution of the matrix region.

not conduct water, inducing a drastic drop in cumulative infiltration. In contrast, the hydraulic functions predicted by BEST-2K involve a matrix region that sustains enough water infiltration at −30 mm. For the other cases, no logical trends were found. It was found that BEST-1K fit only the Beerkan data and thus offers the best fits for Beerkan data, whereas BEST-2K offers the best accuracy considering both TI and Beerkan experiments. For real DP soils, BEST-1K clearly provides a better consistency with regard to the modeling of the two cumulative infiltrations.

Discussion and Limitations

We have validated the BEST-2K methods using analytically generated and real experimental data acquired in the field and highlighted the following crucial points. Under optimal conditions of use (error-free experimental data), both BEST-2K-A and BEST-2K-B provide results close to the target curves. The analytical sensitivity analysis proves that the robustness of estimates with respect to erroneous inputs varies with the selected method. BEST-2K-A seems more robust, in particular, with regard to the volume fraction occupied by the fast-flow region, w_f. Even though the estimates of the hydraulic parameters may differ from the target values, the prediction of the hydraulic functions match closely with the target hydraulic functions. Consequently, BEST-2K-A is more suitable when w_f cannot be determined properly. BEST-2K-A and BEST-2K-B are sensitive to the accuracy of the water measurements, including the water content at the end of the TI experiment and the bulk saturated water content, which is derived from the bulk density. Water contents should be measured with a minimal uncertainty. Regarding the cumulative infiltration, the experimental devices should be chosen so as to allow sufficient time to reach steady state while describing the transient state with enough precision. The test of the BEST-2K methods with experimental data demonstrated that the cumulative infiltration obtained with the tension infiltrometer must be long enough to reach steady state for the matrix. For the Beerkan experiment, the occurrence of the fast-flow region may increase the infiltration rate and reduce the duration of the transient state at the same time, thus requiring an experimental setup to enable precise definition of the cumulative infiltration over a very short duration. Last, the analytical calculations proved that any of the BEST methods (Slope, Intercept, or Steady) should be capable of producing identical results, with the exception of a risk of failure for BEST Slope and BEST Intercept when the transient state is not properly described.

Despite the validation of BEST-2K with both numerical and experimental data, some limitations remain. First, half of the experimental data were not predicted to indicate DP behavior; this finding suggests that either the sampled soils were SP soils or that the BEST-2K method was unable to detect their DP behaviors.

Several opportunities for improvement emerged. First, we need to improve our ability to detect DP behavior. In general, DP behaviors induce a sharp increase in the hydraulic conductivity (Angulo-Jaramillo et al., 2016), with differences of various orders of magnitude between unsaturated and saturated hydraulic conductivity (e.g., Watson and Luxmoore, 1986). However, it may be difficult to distinguish between SP systems with high saturated hydraulic conductivity and very low water retention by capillarity and soils that effectively exhibit DP behaviors. Indeed, both types of soils may experience a large increase in water content and hydraulic conductivity close to saturation, even if the increase is expected to be even larger for SP soils (see comparison of BEST-2K and BEST-1K above). For this objective, more detailed information provided by multitension experiments could enhance our ability to distinguish between SP and DP systems, as suggested by

Table 4. Values of the hydraulic parameters† for the sampled soils at the forest, pasture, and orchard sites.

Site	Domain	w	θ_r	θ_s	n	η	K_s	$\lvert h_g \rvert$
		%	——— $cm^3\ cm^{-3}$ ———				mm min^{-1}	mm
Forest 1	matrix	61.3	0	0.509	2.198	13.1	3.59×10^{-2}	98.5
	fracture	38.7	0	0.752	2.230	11.7	2.14×10^{0}	12.5
Forest 2	matrix	61.3	0	0.509	2.198	13.1	3.56×10^{-2}	76.2
	fracture	38.7	0	0.752	2.230	11.7	2.89×10^{0}	10.1
Pasture 1	matrix	93.8	0	0.370	2.127	18.8	6.54×10^{-2}	9.23
	fracture	6.2	0	0.552	2.688	5.91	3.58×10^{0}	149.8
Pasture 2	matrix	93.8	0	0.370	2.127	18.8	5.86×10^{-2}	4.92
	fracture	6.2	0	0.552	2.688	5.91	3.26×10^{0}	260.7
Orchard 1	matrix	72.9	0	0.497	2.172	14.7	2.50×10^{0}	16.5
	fracture	27.1	0	0.715	2.384	8.21	4.10×10^{1}	29.0
Orchard 2	matrix	62.6	0	0.496	2.172	14.6	1.27×10^{0}	35.0
	fracture	37.4	0	0.740	2.384	8.36	1.39×10^{1}	2.68

† w, volume percentage occupied by the medium; θ_r, residual water content; θ_s, saturated water content; n, shape parameter for the water retention curve; η, exponent of the relative hydraulic conductivity; K_s, saturated hydraulic conductivity; $\lvert h_g \rvert$, scale parameter for water pressure head

Lassabatere et al. (2014). Further research, including numerical or experimental investigations, is needed to properly define the values of the water pressure heads to be imposed for the detection of DP behaviors.

Second, the accuracy of the BEST-2K method that estimates the shape parameters from the bulk PSD should be investigated more deeply. The impact of erroneous estimates of the shape parameter on the bulk hydraulic curves should be investigated in more detail. In addition to the errors resulting from the PTFs, decomposing the PSD into bimodal curves and assigning each mode to the matrix or fast-flow regions may be questionable. Indeed, if it is clear that soil structure may be induced by the soil texture (with the development of larger pores around the largest particles), other external factors may impact the soil structure. Bioturbation and shrinkage due to wetting–drying or freeze–thaw cycles may also create macropore systems, even in a soil that exhibit a unimodal PSD. In this situation, the derivation of shape parameters from the PSD may be questionable, particularly for the fast-flow region.

Third, some parameters of the DP system have yet to be estimated. The proposed methodology does not provide a specific way to estimate the volume fraction occupied by the fast-flow region, w_f. The determination of w_f remains very tricky and may require additional experiments. Micromorphological images could be used to estimate w_f from image analysis (Kodešová et al., 2009). Tracer experiments may also be used to distinguish the porosity that is easily accessible by solutes (which correspond to the fast-flow region) from the inaccessible porosity (which correspond to stagnant water zones in the matrix) (Kodešová et al., 2010, 2012). The use of dyes in the field may also help in the detection of preferential pathways and the characterization of the volume of soil affected by preferential flow (Cey and Rudolph, 2009; Cey et al., 2009). Besides w_f, the BEST-2K methods also do not provide any estimate of the interfacial hydraulic conductivity $K_{s,a}$, which determines the water exchange between the matrix and fast-flow regions. In fact, Lassabatere et al. (2014) suggested that water exchange does not change water infiltration into the DP porous medium for any water pressure head imposed at the soil surface. In other words, whatever the value of $K_{s,a}$, the TI and Beerkan experimental data are identical, which leads to similar characterization by the BEST-2K methods. However, the numerical results of Lassabatere et al. (2014) require additional validation by experimental data. Further numerical and experimental studies are needed (i) to investigate more deeply the effect of nonequilibrium between the matrix and fast-flow regions and related effects on water infiltration, and (ii) to design a proper strategy to estimate $K_{s,a}$. As for w_f, additional laboratory and field experiments, such as tracer or dye experiments, may be necessary to better describe the water exchange between the matrix and fast-flow regions to obtain more insight on $K_{s,a}$ and the effect of nonequilibrium between these regions on the flow processes.

Last, the quality of BEST-2K also strongly depends on the efficiency of BEST-1K in treating cumulative infiltrations obtained for the matrix and fast-flow regions. BEST-1K methods may lead to unreliable results in the case of nonattainment of steady-state conditions or inappropriate descriptions of the transient state. This was probably the case with our experimental data. We obtained higher values of the scale parameter for water pressure head $|h_g|$ for the fast-flow region, which is not physically realistic because it suggests that more water retention by capillarity occurs in the fast-flow region than in the matrix region. The imprecise descriptions of cumulative infiltration, with a poor description of the transient state for the fast-flow region, and the nonattainment of a steady state in the matrix region are probably the explanations for the errors found in estimation of the scale parameter $|h_g|$. In future studies, the use of precise, simple, and inexpensive automatic monitoring systems, such as that proposed by Di Prima (2015), could improve the quality of cumulative infiltration measurements over short durations. Similar devices could be designed for the application of tension infiltrometers that would allow infiltration experiments to last long enough to attain steady-state conditions.

Conclusion

This study developed a new method (BEST-2K) for the characterization of DP soils on the basis of the BEST-1K methods previously developed for SP soils. BEST-2K needs only raw data (PSD and initial and final water contents) and the cumulative infiltrations obtained at two different water pressure heads, i.e., −30 mm to activate only the matrix and 0 mm to activate the entire pore network. With these data, BEST-2K provides a full characterization of DP soils. Two methods were presented. BEST-2K-A uses the two water contents measured at −30 and 0 mm to derive the saturated water contents of the matrix and fast-flow regions. Accurate water measurements are then required. On the other hand, BEST-2K-B is a simpler alternative that equates both local water contents to the soil bulk porosity. BEST-2K-B may be used when the uncertainties in the water measurements are too high. The two methods were validated using both analytical and real experimental data. In the absence of clear evidence for the selection of one or the other method, the use of both methods and subsequent merging of the obtained results may be recommended.

The tests of the two proposed methods highlighted their strengths and weaknesses. Notwithstanding the required research for additional improvements, the BEST-2K method marks a useful first step toward the characterization of DP soils. The method requires only simple water infiltration tests and soil characteristics, thus minimizing time and cost requirements and providing an exhaustive characterization of DP soils. Its association with the regular BEST-1K methods may offer a very interesting tool for the hydraulic characterization of soils prone to preferential flow. Further research activities will be conducted to enhance this approach for the detection and quantification of preferential flow in soils.

List of Symbols

BEST-1K parameters

θ_r	residual water content
θ_s	saturated water content
K_s	saturated hydraulic conductivity
h_g	scale parameter for water pressure head
n	shape parameter for water retention function
η	shape parameter for hydraulic conductivity function
S	sorptivity
ε	porosity
s	fractal dimension
p_m	shape index related to water retention function
p_M	textural shape index related to particle size distribution
p	tortuosity parameter
c_p	shape parameter for cumulative infiltration
$I_{O(2)}(t)$	transient-state approximate expansion for cumulative infiltration
$I_{+\infty}(t)$	steady-state approximate expansion for cumulative infiltration
$q_{O(2)}(t)$	transient-state approximate expansion for infiltration rate
$q_{+\infty}(t)$	steady-state approximate expansion for infiltration rate
A, B, C	coefficients for the approximate expansions
q_s^{exp}	steady-state infiltration rate (slope of the steady state asymptote)
b_s^{exp}	intercept of the steady-state asymptote
S_{opt}	optimized value for sorptivity
$K_{s,opt}$	optimized value for saturated hydraulic conductivity
t_{max}	maximum time for the validity of the transient-state approximate expansion

BEST-2K parameters

w_f	volume fraction of the dual-permeability soil occupied by the fast-flow region
θ_{2K}	bulk water content for the dual-permeability soil
$\theta_{s,2K}$	bulk saturated water content for the dual-permeability soil
θ_m, θ_f	local water contents in the matrix and the fast-flow regions
$\theta_{s,m}, \theta_{s,f}$	local saturated water contents for the matrix and the fast-flow regions
$\theta_{r,m}, \theta_{r,f}$	local residual water contents for the matrix and the fast-flow regions
K_{2K}	bulk hydraulic conductivity for the dual-permeability soil
$K_{s,2K}$	bulk saturated hydraulic conductivity for the dual-permeability soil
K_m, K_f	local hydraulic conductivities for the matrix and the fast-flow regions
$K_{s,m}, K_{s,f}$	local saturated hydraulic conductivities for the matrix and the fast-flow regions
$h_{g,m}, h_{g,f}$	scale parameter for water pressure head for the matrix and the fast-flow regions
n_m, n_f	shape parameter of the local water retention function of the matrix and the fast-flow regions
η_m, η_f	shape parameter of the local hydraulic conductivity function for the matrix and the fast-flow regions
ρ_d, ρ_s	dry bulk density and soil particle density
PSD	bulk particle size distribution
PSD_m, PSD_f	local particle size distribution for the matrix and the fast-flow regions
FF_{2K}	bulk cumulative particle size distribution
τ_f	fraction related to the contribution of the fast-flow region to the bulk particle size distribution
$D_{g,m}, D_{g,f}$	average diameter of the particles of the matrix and the fast-flow regions
N_m, N_f	textural parameters for the matrix and the fast-flow regions
θ_{TI}	bulk water content at the end of TI experiments
$\theta_{TI,m}, \theta_{TI,f}$	local water content in the matrix and the fast-flow regions at the end of TI experiments
$\theta_{0,TI}, \theta_{0,B}$	bulk initial water content for TI and Beerkan experiments
$\theta_{0,m}, \theta_{0.f}$	local initial water contents for the matrix and the fast-flow regions
I_B	bulk cumulative infiltration related to Beerkan experiment
t_B	time dataset for the Beerkan experiment
I_{TI}	bulk cumulative infiltration related to TI experiment
t_{TI}	time dataset for the TI experiment
$I_{B,m}, I_{B,f}$	cumulative infiltration for Beerkan experiments sampling only the matrix and the fast-flow regions
$I_{B,m}(t_B)$	cumulative infiltration for Beerkan experiments sampling only the matrix computed for time dataset t_B
$I_{3D,2K}(t)$	model for the computation of cumulative infiltrations into dual-permeability soils for TI and Beerkan experiments
r_d	radius of the source for water infiltration experiments
S_m, S_f	computed sorptivities for the matrix and the fast-flow regions
D_m, D_f	water diffusivity for the matrix and the fast-flow regions
$\beta_m, \gamma_m, \beta_f, \gamma_f$	infiltration constants related to quasi-exact implicit model and related approximate expansions for the matrix and fast-flow regions
$r_{g,m}, r_{g,f}$	local averaged pore size for the matrix and the fast-flow regions
σ_{aw}	surface tension of the air/water interface
β_c	contact angle
ρ_w	water density
g	gravitational acceleration constant
$Er\theta_0, Er\theta_s, ErI$	errors of BEST-2K preprocessing function for the computation of initial water contents, saturated water contents, and cumulative infiltration, respectively

Acknowledgments

We wish to thank the French National Research Agency (ANR) for its contribution to the funding of the INFILTRON Project (ANR-17-CE04-0010) and, in particular, this work and for providing scientific supervision of the research. We also thank the Field Observatory in Urban Water Management (OTHU) for technical and scientific support. We would like to thank the associate editor, Majdi Abou Najm, and the reviewers for their excellent suggestions and contributions.

These were crucial for the improvement of the manuscript, and we greatly appreciate their advice. We also thank R. Marrosu for his assistance in the field activity.

References

Arya, L.M., and J.F. Paris. 1981. A physicoempirical model to predict the soil moisture characteristic from particle-size distribution and bulk density. Soil Sci. Soc. Am. J. 45:1023–1030. doi:10.2136/sssaj1981.03615995004500060004x

Angulo-Jaramillo, R., V. Bagarello, M. Iovino, and L. Lassabatere. 2016. Infiltration measurements for soil hydraulic characterization. Springer, Berlin. doi:10.1007/978-3-319-31788-5

Bagarello, V., S. Di Prima, and M. Iovino. 2014. Comparing alternative algorithms to analyze the Beerkan infiltration experiment. Soil Sci. Soc. Am. J. 78:724–736. doi:10.2136/sssaj2013.06.0231

Braud, I., D. De Condappa, J.M. Soria, R. Haverkamp, R. Angulo-Jaramillo, S. Galle, and M. Vauclin. 2005. Use of scaled forms of the infiltration equation for the estimation of unsaturated soil hydraulic properties (the Beerkan method). Eur. J. Soil Sci. 56:361–374. doi:10.1111/j.1365-2389.2004.00660.x

Brooks, R., and A. Corey. 1964. Hydraulic properties of porous media. Hydrol. Pap. 3. Colo. State Univ., Fort Collins.

Burdine, N.T. 1953. Relative permeability calculations from pore size distribution data. J. Pet. Technol. 5(03):71–78. doi:10.2118/225-G

Carsel, R.F., and R.S. Parrish. 1988. Developing joint probability distributions of soil water retention characteristics. Water Resour. Res. 24:755–769. doi:10.1029/WR024i005p00755

Cey, E.E., and D.L. Rudolph. 2009. Field study of macropore flow processes using tension infiltration of a dye tracer in partially saturated soils. Hydrol. Processes 23:1768–1779. doi:10.1002/hyp.7302

Cey, E.E., D. Rudolph, and J. Passmore. 2009. Influence of macroporosity on preferential solute and colloid transport in unsaturated field soils. J. Contam. Hydrol. 107:45–57. doi:10.1016/j.jconhyd.2009.03.004

Di Prima, S. 2015. Automated single ring infiltrometer with a low-cost microcontroller circuit. Comput. Electron. Agric. 118:390–395. doi:10.1016/j.compag.2015.09.022

Di Prima, S., L. Lassabatere, V. Bagarello, M. Iovino, and R. Angulo-Jaramillo. 2016. Testing a new automated single ring infiltrometer for Beerkan infiltration experiments. Geoderma 262:20–34. doi:10.1016/j.geoderma.2015.08.006

Durner, W. 1994. Hydraulic conductivity estimation for soils with heterogeneous pore structure. Water Resour. Res. 30:211–223. doi:10.1029/93WR02676

Gee, G.W., and J.W. Bauder. 1986. Particle-size analysis. In: A. Klute, editor, Methods of soil analysis. Part 1. Physical and mineralogical methods. SSSA Book Ser. 5. SSSA and ASA, Madison, WI. p. 383–411. doi:10.2136/sssabookser5.1.2ed.c15

Gerke, H.H., and M.Th. van Genuchten. 1993. A dual-porosity model for simulating the preferential movement of water and solutes in structured porous-media. Water Resour. Res. 29:305–319. doi:10.1029/92WR02339

Gonzalez-Sosa, E., I. Braud, J. Dehotin, L. Lassabatere, R. Angulo-Jaramillo, M. Lagouy, et al. 2010. Impact of land use on the hydraulic properties of the top soil in a French catchment. Hydrol. Processes 24:2382–2399. doi:10.1002/hyp.7640

Haverkamp, R., P.J. Ross, K.R.J. Smettem, and J.-Y. Parlange. 1994. Three-dimensional analysis of infiltration from the disc infiltrometer: 2. Physically-based infiltration equation. Water Resour. Res. 30:2931–2935. doi:10.1029/94WR01788

Kodešová, R., K. Němeček, V. Kodeš, and A. Žigová. 2012. Using dye tracer for visualization of preferential flow at macro- and microscales. Vadose Zone J. 11(1). doi:10.2136/vzj2011.0088

Kodešová, R., J. Šimůnek, A. Nikodem, and V. Jirků. 2010. Estimation of the dual-permeability model parameters using tension disk infiltrometer and Guelph permeameter. Vadose Zone J. 9:213–225. doi:10.2136/vzj2009.0069

Kodešová, R., N. Vignozzi, M. Rohošková, T. Hájková, M. Kočárek, M. Pagliai, et al. 2009. Impact of varying soil structure on transport processes in different diagnostic horizons of three soil types. J. Contam. Hydrol. 104:107–125. doi:10.1016/j.jconhyd.2008.10.008

Kutilek, M., and D.R. Nielsen. 1994. Soil hydrology. Catena Verlag, Cremlingen, Germany.

Lassabatere, L., R. Angulo-Jaramillo, J.M. Soria Ugalde, R. Cuenca, I. Braud, and R. Haverkamp. 2006. Beerkan estimation of soil transfer parameters through infiltration experiments: BEST. Soil Sci. Soc. Am. J. 70:521–532. doi:10.2136/sssaj2005.0026

Lassabatere, L., R. Angulo-Jaramillo, J.M. Soria-Ugalde, J. Šimůnek, and R. Haverkamp. 2009. Numerical evaluation of a set of analytical infiltration equations. Water Resour. Res. 45:W12415. doi:10.1029/2009WR007941

Lassabatere, L., D. Yilmaz, X. Peyrard, P.E. Peyneau, T. Lenoir, J. Šimůnek, and R. Angulo-Jaramillo. 2014. New analytical model for cumulative infiltration into dual-permeability soils. Vadose Zone J. 13(12). doi:10.2136/vzj2013.10.0181

Lenhard, R.J., J.H. Dane, and M. Oostrom. 2005. Immiscible fluids. In: D. Hillel, editor, Encyclopedia of soils in the environment. Elsevier, Amsterdam. p. 239–247.

Parlange, J.-Y. 1975. On solving the flow equation in unsaturated soils by optimization: Horizontal infiltration. Soil Sci. Soc. Am. J. 39:415–418. doi:10.2136/sssaj1975.03615995003900030019x

Rieu, M., and G. Sposito. 1991. Fractal fragmentation, soil porosity, and soil water properties: II. Applications. Soil Sci. Soc. Am. J. 55:1239–1244. doi:10.2136/sssaj1991.03615995005500050007x

Schaap, M.G., F.J. Leij, and M.Th. van Genuchten. 2001. ROSETTA: A computer program for estimating soil hydraulic parameters with hierarchical pedotransfer functions. J. Hydrol. 251:163–176. doi:10.1016/S0022-1694(01)00466-8

Smettem, K.R.J., J.-Y. Parlange, P.J. Ross, and R. Haverkamp. 1994. Three-dimensional analysis of infiltration from the disc infiltrometer: 1. A capillary-based theory. Water Resour. Res. 30:2925–2929. doi:10.1029/94WR01787

Sutera, S.P., and R. Skalak. 1993. The history of Poiseuille's law. Annu. Rev. Fluid Mech. 25:1–20. doi:10.1146/annurev.fl.25.010193.000245

Timlin, D.J., L.R. Ahuja, and M.D. Ankeny. 1994. Comparison of three field methods to characterize apparent macropore conductivity. Soil Sci. Soc. Am. J. 58:278–284. doi:10.2136/sssaj1994.03615995005800020003x

van Genuchten, M.Th. 1980. A closed-form equation for predicting the hydraulic conductivity of unsaturated soils. Soil Sci. Soc. Am. J. 44:892–898. doi:10.2136/sssaj1980.03615995004400050002x

Watson, K.W., and R.J. Luxmoore. 1986. Estimating macroporosity in a forest watershed by use of a tension infiltrometer. Soil Sci. Soc. Am. J. 50:578–582. doi:10.2136/sssaj1986.03615995005000030007x

Yilmaz, D., L. Lassabatere, R. Angulo-Jaramillo, D. Deneele, and M. Legret. 2010. Hydrodynamic characterization of basic oxygen furnace slag through an adapted BEST method. Vadose Zone J. 9:107–116. doi:10.2136/vzj2009.0039.